AUTOMATIC OR COUPLED CONTROL SURFACES FOR AIRCRAFT

Thesis by

James B. Kendrick

In Partial Fulfillment of the Requirements

for the Degree of

Aeronautical Engineer

California Institute of Technology

Pasadena, California

1951

Acknowledgments

The author wishes to acknowledge his gratitude to the late Dr. Mac Short of Lockheed Aircraft Corporation, whose foresight and confidence made this investigation possible; to Mr. Bernard Rasof and Drs. H. J. Stewart, N. O. Myklestad, and C. C. Lin, of the California Institute of Technology, for helpful aid regarding some of the mathematical interpretations; to Prof. O. C. Koppen and Mr. Ben Drisko, of the Massachusetts Institute of Technology, for encouragement and many useful suggestions; and his co-workers at Lockheed, Dr. F. W. Ross and Mr. Ray Patterson, who helped to conduct many of the wind-tunnel tests on the coupled fin and rudder.

Automatic or Coupled Control Surfaces for Aircraft

Abstract

An improved method of aircraft stabilization is described, with wind tunnel test results and stability criteria, and suggestions for use in aircraft design. The method utilizes a new type of control surface consisting of a mechanically coupled fin and rudder, which converts the tail surface into an automatic servo control.

Theory and wind tunnel tests show that the lift curve slope of the tail, $dC_L/d\alpha$, may be increased by six times or more in this way, using reasonable but not extraordinary care with manufacturing methods and tolerances.

The dynamic stability criteria are given and compared with wind tunnel tests for nine different balance conditions of two models tested on a swinging arm in the wind tunnel. Four out of the nine cases were stable, and the stability criteria give the correct indication in every case.

Stability analysis is used to indicate the effect of coupled surfaces on the lateral and longitudinal motion of a conventional transport airplane. With the regular control surfaces, this airplane has a spiral divergence, "dutch roll," and a poorly damped long-period longitudinal oscillation. With the coupled tail surfaces, having a very moderate increase in static stability over that of the fixed surfaces, all of the above objectionable characteristics are eliminated, and the resulting airplane modes are shown to be either aperiodic or damped periodic motion of very short period.

The application of such control surfaces to real airplanes appears to be feasible with little change in the design procedure. Several examples are given of coupled tail designs for different kinds of aircraft. The principle is also shown to be applicable to supersonic vehicles. The economic advantages of airplanes equipped with such stabilizers, together with the success of the analysis and test work to date, suggest that this device is worthy of further development and application to aircraft.

Table of Contents

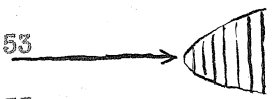

List of Figures and Tables

Fig.1. Model of Coupled Fin and Rudder

To assemble model: Paste this sheet to thin cardboard.

Cut out tail surface as instructed below.

Hinge-mount tail at base of fin with tape.

Make rudder hinge with tape.

Place a piece of wire along node line from A to C. (about .040 inch diam. wire). Apply tape at A & B. This wire represents the rudder spar, which extends down into the fuselage to the point of attachment of the controls at C.

For brief demonstration, follow directions below.

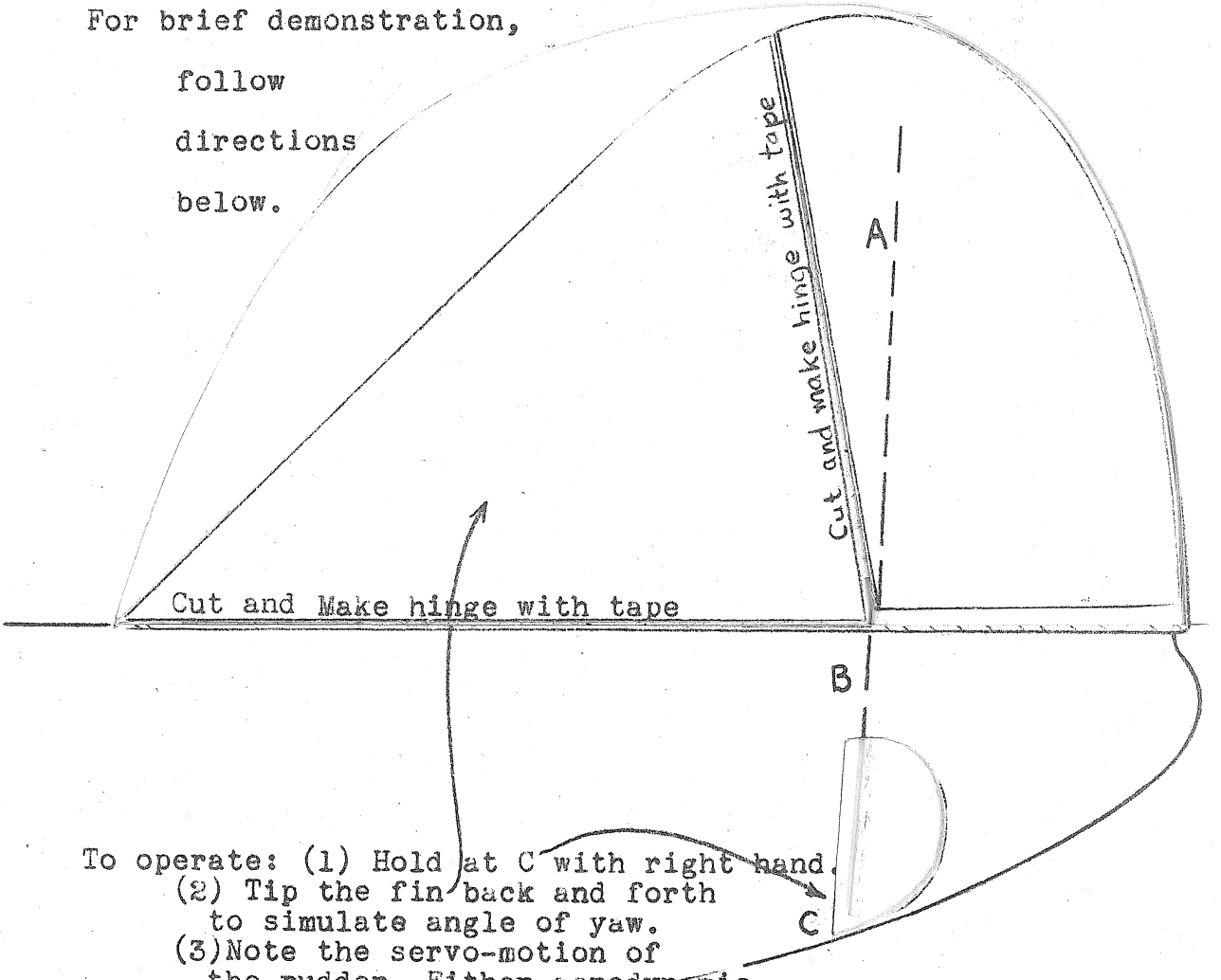

To operate: (1) Hold at C with right hand.
(2) Tip the fin back and forth to simulate angle of yaw.
(3) Note the servo-motion of the rudder. Either aerodynamic or inertia forces acting on the tail will cause the rudder to move in the proper direction to correct the condition.
(4) Twist rudder spar at C for control or trim.

I. Introduction

The inherent stability of airplanes with free controls has long been the subject for intensive theoretical and experimental research. At best the airplane is a rather loosely stabilized device, in which the natural aerodynamic damping is a small percentage of critical damping; hence, disturbances cause oscillations which persist for several cycles before damping out. In rough air, the attenuation of such motions may be so poor that the airplane appears to wallow incessantly. Man's inventive genius has devised a mechanical aid in the autopilot, by means of which the controls are actuated in proper phase and modulus to give the impression of critically damped motion.

Test pilots and engineers have an insatiable desire to provide airplanes with more and more inherent stability, to make them easier to fly with less attention from the pilot and less fatigue after extended flight. Designers appreciate this desire for more stability and strive to satisfy it to a greater degree on each succeeding new design. But unfortunately the goal is always a little beyond, since, with each improvement, the standards are raised again. The pilot returns from a test flight to report that the new prototype is "a hundred times easier to fly than current models," but the next day he convinces the engineer that there is still room for improvement before the airplane can fly "hands-off" as well as when directed by the autopilot. By such constant endeavor, seeming progress is being made toward the goal of "perfect inherent stability;" i.e., a smoother ride with almost critically damped disturbances.

The idea of coupled surfaces (cf. Fig. 1, frontispiece) was conceived under the conditions just described. After several new models had been produced with larger and larger vertical tails (cf. Fig. 2), and with

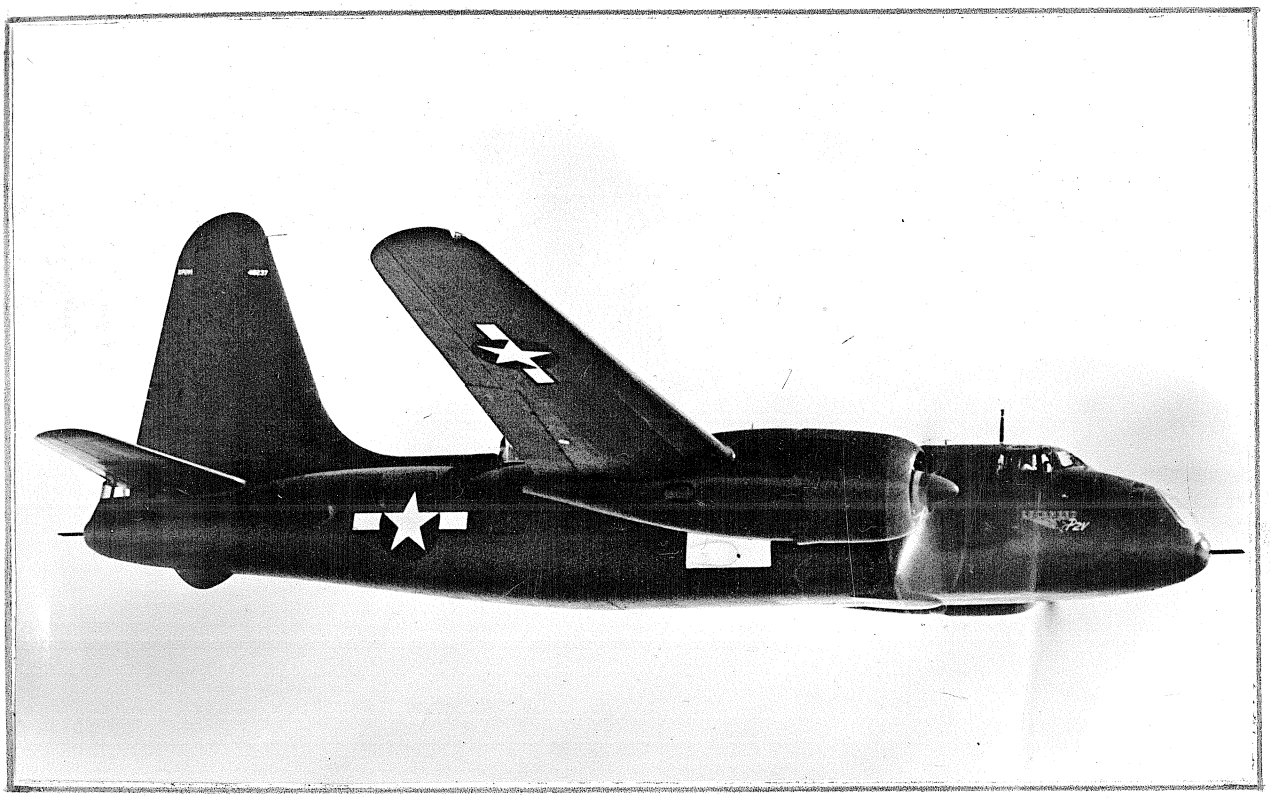

Fig. 2. Lockheed P2V "Neptune" Patrol Bomber

Observation: As airplanes grow more useful, vertical tails grow larger.

Thesis: The present aerodynamic development permits the attainment of more nearly perfect inherent stability with control surfaces of moderate area.

"the boss" specifying that the next model should have "much higher maximum lift and more inherent stability," the designer called upon inspiration to bring forth a solution. The idea of automatic or coupled control surfaces soon presented itself, and although there were many suggestions of uncertainties at that early date, it seemed worthy of a trial.

The subsequent development of coupled surfaces described herein is cited as an example of the analytical approach to experimental development. From the first conception of the idea, it had been the author's intention that analysis should lead the way for experimental work. After the development had progressed to a point where its success looked hopeful, great demands were made upon theory to clarify the dynamic stability problem, since further progress seemed impractical by any other method. Thus analysis was forced to take the lead, with results which will be left to the reader's judgment.

The work appeared to be of sufficient theoretical scope and technical importance to the aircraft industry to warrant the expenditure of considerable time and energy in its solution. The first attempt to solve the dynamic problem and specify a design procedure, though fairly successful (cf. Ref. 1), was disappointing in that the procedure was so complicated as to seem of dubious reliability. Further patience was rewarded with the theory presented herein, which seems to be simple, practical, and readily applicable to current aerial vehicles. This work, augmented by several examples of applications to modern airplane designs including supersonic missiles, appeared to be of suitable nature for submission as an academic thesis, for which purpose it is now respectfully presented.

II. Discussion of Airplane Stability

A. Formulation of Stability Concepts

Airplane stability has been a subject for theoretical and experimental development work for half a century. Lanchester (cf. Ref. 2) first disclosed the nature of the dynamic problems involved in flying machines and the complexity of the methods of solving such problems. Many willing hands then contributed to the streamlining of the procedure for conducting such analyses, Bairstow, Glauert, and Hunsaker having presented comprehensive reports on longitudinal and latem/ stability analysis. Other exponents of the analytical approach to the problem, such as Koppen, Weick, and Zimmerman did much to acquaint designers and engineers with the methods for determining the stability characteristics by analysis prior to the airplane test flights. In turn, engineers like Root, Schairer, Johnson, Koppen, Weick and many others have been very successful in utilizing such theoretical methods to bring a higher degree of perfection to airplane stability characteristics.

Complementary to the analytical approach to the stability problem, wind-tunnel and flight tests of the airplane have progressed toward more accurate determination of stability characteristics under various conditions of power, lift, and altitude. The interpretation and correction of eccentricities appearing in wind-tunnel tests have led to improvements in airplane design which, because of the complexity of the problem, would never have been possible by analytical or flight-test methods alone.

Fortunately the dynamics of present-day airplanes is not far different from that of the Wright Brothers machine. The modes of motion which Lanchester discussed are still predominant, and the same general

methods apply to their mathematical treatment. Hence, it has been possible to develop empirical criteria having the nature of static requirements which, if satisfied, would insure that the dynamic behavior of the airplane would be satisfactory (cf. Ref. 3). Such quasi-static criteria have been of great benefit in simplifying the engineers' problems; thus the design process could be expedited and the airplane constructed and flown before the novelty of its combination of speed, control, stability, and detail design would have fallen into obsolescence.

By these methods of design formulation in which each new model is critically examined by a host of pilots and other interested persons whose opinions were integrated by natural processes and made known to the designer, many of the present criteria have been reached. For example, the ratio of tail area to wing area has gradually increased through the years because the requirements of speed, center-of-gravity range, and high lift have so extended the demand for higher stability and trim that it was impractical or uneconomical to do otherwise. Mechanical or electronic autopilots are available which are normally capable of flying the airplane much better than the human pilot, but the field of usefulness of such devices is limited. There will always be a predominance of man-piloted airplanes; hence, the necessity of providing the best designs for that purpose, which will require as little effort and attention as possible.

B. Design Factors Regarding Stability

In the case of lateral stability, most airplanes exhibit three modes of motion at speeds above the stall (cf. Sec. V-B): a well-damped subsidence in roll, a spiral motion, and an oscillation in roll and yaw. The vertical tail provides static stability, damping of yaw, and directional trim for unsymmetrical yawing moments. At stalling speeds, the

damping of roll becomes unstable, and a vertical tail of great power is needed to prevent the airplane from spinning. The maximum requirement for vertical tails is that a certain product of area times $dC_L/d\alpha$ (cf. nomenclature) should be available in case of emergency, in order to prevent excess yaw in case of a sudden engine failure on a multi-engine plane, or to maintain the wings level in case of a stall.

The longitudinal motion of most airplanes consists of two oscillatory modes (cf. Sec. V-B), one of short period in which inertia and elastic effects predominate, and another of long period which involves change in speed and altitude. The requirements for horizontal tails are that the pilot shall be able to land the airplane conveniently by use of the manual elevator control, and the airplane shall have satisfactory trim characteristics throughout a wide range of speeds, centers of gravity, and power and flap settings and shall damp out the long-period mode in a reasonable time. The design requirements for horizontal tails then reduce to the selection of area times C_L for control and trim (with appropriate stick forces); area times $dC_L/d\alpha$ for stability, with good damping characteristics; and an over-all design for stalling characteristics and riding comfort.

The purpose of this treatise is to describe a method of coupling control surfaces so that they will act as automatic controls, thus increasing by a factor of 4 or more the product of area times $dC_L/d\alpha$. This principle is of great value economically to all types of aircraft from single-engine to multi-engine airplanes, and seems to be applicable to vehicles traveling at all speeds from subsonic to supersonic. A brief consideration of the economic aspects of the problem may be of interest. (cf. Ref. 4 and Appen. A).

D. Description of Coupled Tail

The object of this investigation is to describe a new type of airplane control surface (cf. Fig. 1, frontispiece) that is many times more powerful, as a stabilizing or damping means, than is a fixed surface of equal area. This increase in effectiveness is accomplished in the following manner:

As shown in Fig. 3, the lateral force F produced by angle of yaw ψ causes the vertical surface to tip through the angle γ about its base. Coupling link L between the rudder and a fixed point (preferably inside the fuselage) causes the rudder to deflect through angle β. The rudder deflection acts in the proper direction to reduce the angle of yaw ψ. This procedure has converted the control surface into an automatic servo control.

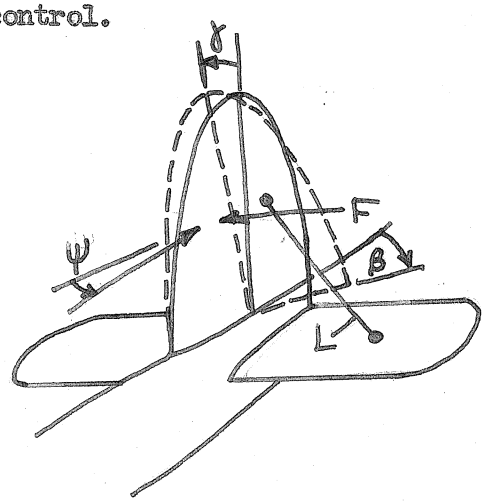

Fig. 3. General View of Coupled Fin and Rudder.

As a free control, the effect of the coupled tail upon the airplane is an improvement over the action of a conventional surface of much larger area. It may be adapted to manual control in the normal manner, but one should note that the maximum lift or moment will be no greater than that of a conventional surface, even though the slope of

the lift curve is many times as great. When the coupled tail is considered as a vertical tail surface for an airplane, there are several direct advantages to be gained by use of this principle, as follows: to improve the directional stability with moderate tail area; to insure satisfactory stability and stall characteristics with shorter and/or smaller tail; to provide high free-control stability at wide angles of yaw, for spin prevention; to permit weight and performance saving by reduction in the tail area. The principle has good possibilities for use in two-control operation, where high directional stability is necessary.

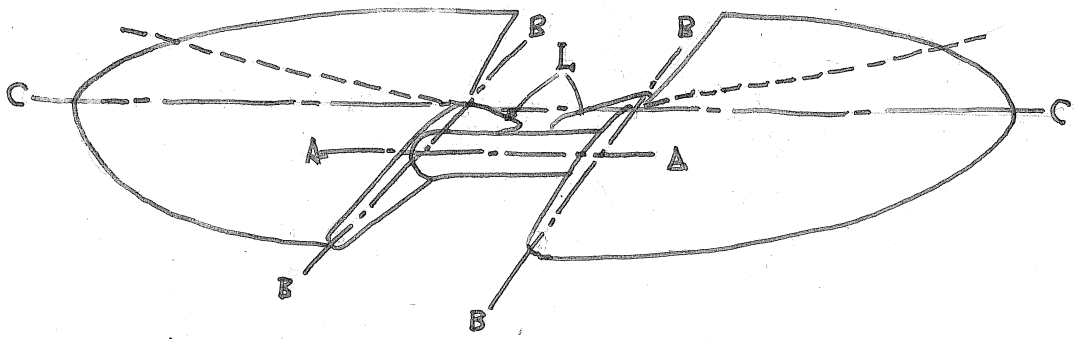

Fig 4. Horizontal Tail Application of Coupled Surfaces

Considered as a horizontal tail for a small airplane, the coupled surfaces might appear as in Fig. 4, the entire surface moving on A-A actuated by the longitudinal control system. Each of the tail half-panels tilts on B-B when the angle of attack changes. The tilt causes movement of the elevator on C-C, actuated by coupling link L or other suitable mechanism. Normal stick control changes the stabilizer setting to give desired air speed or flight-path angle. Trim to a desired air speed may be accomplished by stabilizer adjustment.

After the stabilizer is set for a desired air speed, the high static stability resulting from the coupled elevator will hold that airspeed automatically more closely than with normal stability (cf. Fig. 5). The ability to hold constant air speed is dependent on the value of dC_M/dC_L which the airplane possesses when operating with free controls. The advantages of coupled horizontal surfaces are as follows:

First, improved stability. Proper stability requires the correct ratio of static stability to damping. When the static stability is low,

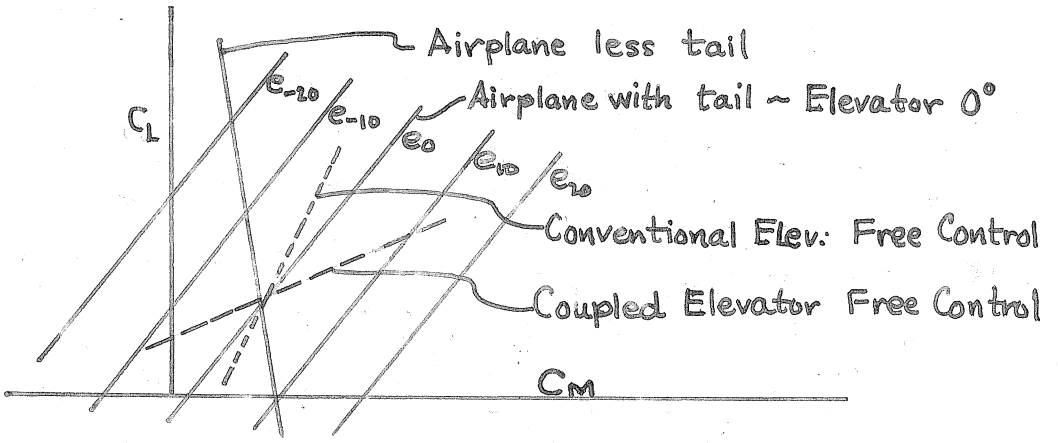

Fig 5. Effect of Coupled Surfaces on Static Longitudinal Stability

variations in c.g. location cause this ratio to change drastically, making it impossible to provide consistent stability characteristics throughout the c.g. range. However, by use of the coupled tail, the static stability may be increased to a point where variations due to c.g. movement have only moderate effect on the stability.

Second, better air speed control. Variations in angle of attack and/or velocity will be quickly corrected by the action of the coupled elevator, which exerts a powerful automatic leading control. The angle of attack α leads the angular velocity by about 1/4 cycle. Variation in α will therefore be corrected promptly by control action. This

feature is in contrast to that of conventional control surfaces, where the elevator motion lags a change in α , thus prolonging the motion.

Third, greater riding comfort in rough air. When an airplane strikes a vertical gust, motion will soon result if the controls are not automatically compensated, to relieve the airplane of the additional unwanted lift. The coupled elevator offers the advantage of gust alleviation by virtue of a favorable inertia effect; hence, the reaction to gusts will be less severe, and the riding comfort should be greater.

Since any servo mechanism is susceptible to a tendency to oscillate unless properly damped, this subject has been carefully studied, and stability criteria are provided for use in design. The resulting surface will return promptly to its original setting when deflected from a trimmed position in an air stream.

Another arrangement of all-movable surfaces (cf. Ref. 5 and Fig. 6) has the forward surface hinged on an axis parallel to the rearward flap surface. Although this method of coupling provides a considerable increase in $dC_L/d\alpha$, it is somewhat less effective than the arrangement of perpendicular hinges described herein, as shown by the following comparison of the effectiveness factor $\eta_s = 1 + \tau \frac{\beta}{\psi}$ for the two methods:

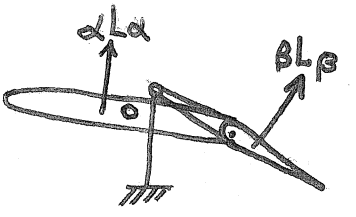

Fig.6 Coupled Surfaces with Parallel Hinge Lines

Method of Coupling	Static Condition	Dynamic Condition	Source of Data
Parallel Hinges (theory	> 2		(cf. Ref. 5)
(test		1.15*	
Perpendicular Hinges (theory	> 8	> 6	
(test	7.6	> 2**	(cf. App. D)

Another point which might be of importance is that the parallel hinge arrangement requires extra balance weights to attain the inertia balance feature of the present design.

The static and dynamic stability will now be developed for the case of a vertical tail surface. This development will likewise serve for horizontal tails and, with slight modifications, may be adapted to the case of ailerons.

* Highest value reported. Larger values may be feasible.

** The dynamic stability theory was not completed when these tests were made.

III. Theory of Coupled Surfaces

A. Static Stability of Coupled Surfaces

The resistance to sideslip $dC_Y/d\psi$ is equal to the sum of the lift due to angle of attack $dC_L/d\alpha$ and lift due to rudder deflection $(dC_L/d\alpha)(d\alpha'/d\beta)(d\beta/d\psi)$, where $d\alpha'/d\beta$ is the change in effective angle of attack of the tail per degree of rudder deflection (normally denoted by τ) and $d\beta/d\psi$ is the rudder deflection per degree of yaw, which may be written β/ψ for small deflections. The sum of these effects is

$$\frac{dC_L}{d\psi} = \frac{dC_L}{d\alpha}\left(1+\tau\frac{\beta}{\psi}\right) \qquad (1)$$

The customary value of tail lift $dC_L/d\alpha$ is thus augmented by the factor $\tau(\beta/\psi)(dC_L/d\alpha)$ produced by the forced rudder deflection. The effect of the coupled tail is therefore $\eta_s = 1+\tau\,\beta/\psi$ times that of a fixed vertical surface of the same area, the term η_s being called the static tail efficiency factor (cf. η_D in Eq. 17). The value of β/ψ may now be derived in terms of the geometrical configuration.

The surface is hinged at the base of the fin (cf. Figs. 1 and 3) and is also provided with the customary rudder hinge. In addition, a nodal line is established diagonally across the rudder by the force of constraint F of the linkage. This node line and the bottom of the fin therefore remain in the plane of symmetry, about which the surface may rotate with a combined tipping motion γ and rudder deflection β, where $R = \gamma/\beta$. The aerodynamic forces and their cp's on the fin and

and rudder are defined as follows:

Four Force System: Force on ↓ / Due to →	ψ	β	Cp on ↓ / Due to →	ψ	β
Fin	ψL_1	βL_2	Fin Measured from r.h.l and t.h.l.	x_1, z_1	x_2, z_2
Rudder	ψL_3	βL_4	Rudder	x_3, z_3	x_4, z_4

It is noted that the forces ψL_1, and βL_2 acting on the fin can produce tipping moment but not rudder hinge moment, because of the restraint exerted by the tip hinge. Their effect is independent of their chordwise c.p. positions on the fin; hence, these forces may be considered to act at the rudder hinge line $(0, z_1)$ and $(0, z_2)$, respectively. Let the new fin forces be $\psi L_1'$ and $\beta L_2'$ after transfer to the r.h.l., but the magnitudes of the forces are unchanged.

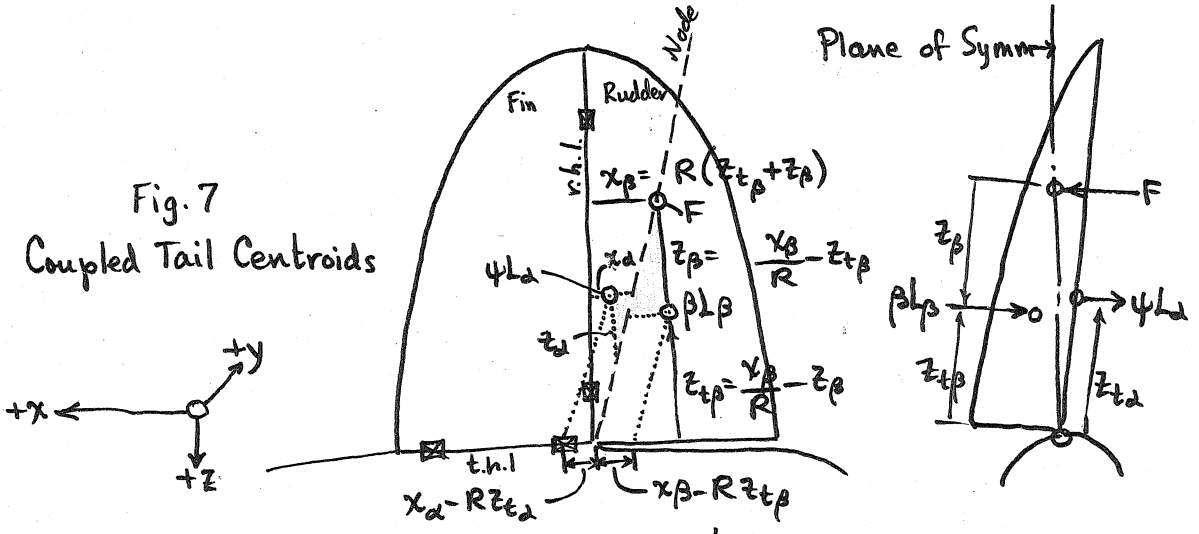

Fig. 7
Coupled Tail Centroids

The sum of the forces due to yaw $(\psi L_1' + \psi L_3)$ is the single force ψL_α, with centroid located at the weighted mean between $(0, z_1)$ and (x_3, z_3), (cf. App. B). Likewise the sum of the rudder produced forces $(\beta L_2' + \beta L_4)$ is βL_β with centroid between $(0, z_2)$ and (x_4, z_4). The action of the two forces ψL_α and βL_β is assumed to be equivalent to that of the four force system mentioned above, insofar as the static and dynamic behavior of the coupled tail are concerned. (cf. Fig. 7).

For simplicity, the two force system will henceforth be used in the analysis, the forces and centroids being as shown in Fig. 7, and defined as follows:

Two Force System	Force on ↓ / Due to →	ψ	β	Centroid of / Due to	ψ	β
	Fin & Rudder	ψL_α	βL_β	Fin & Rudder Coordinates	$x_\alpha, z_{t\alpha}$ from r.h.l.	$x_\beta, z_{t\beta}$ and t.h.l.
	Fin & Rudder	ψL_α	βL_β	Fin & Rudder Coordinates	x_α, z_α from r.h.l.	x_β, z_β and node line.

Static Equilibrium Position. The summation of moments about the rudder hinge line and tip hinge line equals zero for static equilibrium. The equation of constraint $R = \gamma/\beta = x_l/z_l = x_\beta/(z_{t\beta}+z_\beta)$ is also used to reduce the equations.

$$\Sigma M_{rhl} = \psi L_\alpha x_\alpha + \beta L_\beta x_\beta - F z_l = 0$$

$$\Sigma M_{thl} = \psi L_\alpha z_{t\alpha} + \beta L_\beta z_{t\beta} - F z_l = 0$$

Solving for $R = x_l/z_l = \dfrac{\psi x_\alpha + \tau\beta x_\beta}{\psi z_{t\alpha} + \tau\beta z_{t\beta}}$, since $L_\beta = \tau L_\alpha$.

Then the static equilibrium position is found to be (cf. similar triangles in Fig. 7),

$$\frac{\beta}{\psi} = -\frac{1}{\tau}\left(\frac{x_\alpha - R z_{t\alpha}}{x_\beta - R z_{t\beta}}\right) = -\frac{1}{\tau}\frac{z_\alpha}{z_\beta}$$

Other equivalent relationships may be derived from the surface loadings and cp's, (cf. App. C) but the two-force system, with coordinates(x_α, z_α) and (x_β, z_β) measured from the rhl and the node line is simplest in form, and will therefore be used in the analysis which follows. Methods of converting model test data into the design parameters will be found in Appendix B.

Tail Efficiency. The tail efficiency may now be calculated.

$$\eta_s = 1 + \tau\frac{\beta}{\psi} = 1 - \frac{z_\alpha}{z_\beta} = \frac{z_\beta - z_\alpha}{z_\beta} \qquad (2)$$

The case of primary interest when $\eta_s > 1$ is found to occur when $z_\beta > 0$ (cf. Fig. 8) i.e., when the centroid of the rudder-produced forces is aft and below the node line. Under these conditions $\beta/\psi = |z_d|/\tau z_\beta$, which provides the corrective control ($+\beta$ for $+\psi$) as intended from the action of the servo mechanism. A singularity occurs when $z_\beta = 0$, when the centroid of the rudder-produced forces lies on the node line. This condition is to be avoided by adjusting the node line to lie forward of the extreme forward rudder centroid position, $R < R_s$, where $R_s \doteq \frac{x_{4/2}}{z_t}$ determined by experiment. The tail efficiency is then determined by the accuracy of the x_4 and z_t determination.

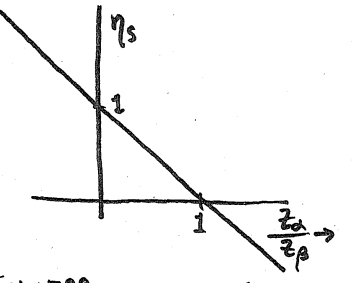

Fig.8 Tail Efficiency vs $\frac{z_d}{z_\beta}$

Since $z_\beta > 0$ for high tail efficiency and $z_d < 0$ for normal tail contours,

$$\eta_s = \frac{|z_d| + z_\beta}{z_\beta}$$

The static tail efficiency is therefore a simple ratio of centroid distances, measured as vertical ordinates with respect to the obtuse node line (cf.Fig. 9).

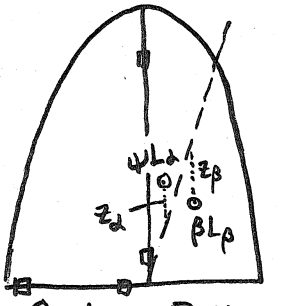

Fig 9 Centroid Positions Determine Tail Efficiency

The novelty of the servo mechanism devised by coupling the two surfaces together may now be realized. The tipping action about the base of the fin provides the error-sensing element, and the tipping moment provides the actuating moment necessary for applying corrective control. These effects work simultaneously to give β proportional to ψ for static conditions, and $\dot{\beta}$ proportional to $\dot{\psi}$ for angular velocities. Inertia effects are also compensated by the servo mechanism since, if

the c. g. is forward and above the node line, the inertia effect of $+\ddot{\psi}$ gives a $+\gamma$ tipping action, which causes $+\beta$ required for corrective control. It is noted that the inertia reaction leads the displacement vector by nearly 1/2 cycle, thus adding an apparent mass effect to the system.

B. Dynamic Stability of Coupled Surfaces

Equations of motion. The motion of the surfaces may be expressed in terms of the angle of yaw ψ and the rudder deflection β . It is now desired to express ψ and β in terms of equations of motion with respect to time, in order to indicate the dynamic behavior of the coupled surfaces. Furthermore, it is desired that a stability criterion may be developed which shows the relative importance of the various aerodynamic and mechanical factors and their proper relationship to insure satisfactory stability. The equations of motion are formulated with the aid of Lagrange's formula (cf. Ref. 6),

$$\frac{d}{dt}\left(\frac{\partial T}{\partial \dot{q}_k}\right) - \left(\frac{\partial T}{\partial q_k}\right) = Q_k \qquad (3)$$

T being the kinetic energy, Q_k the generalized force, and q_k the permissible displacements ψ and β . In fig. 10, the position of any small element ρ_i of mass m_i and coordinates x_i, y_i, z_i , may be expressed in terms of ψ and β , the generalized coordinates.

Note:
Displacements x_i, y_i, z_i are positive forward, to the right, and downward; measured from the cg, plane of symmetry, and the bent node line NoN, resp.

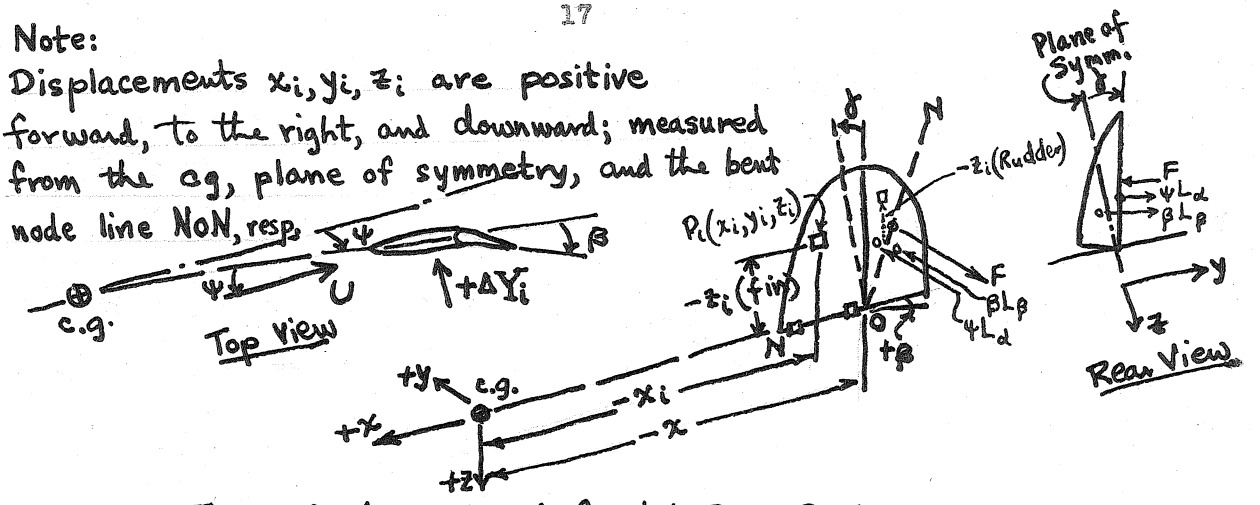

Fig. 10 Configuration of Coupled Fin & Rudder

x_i and z_i will be constant for small values of ψ and β. The lateral displacement y_i is proportional to the angles ψ and γ and the distance of the point i from the airplane c. g. and from the bent node line NoN formed by the tip hinge and the force of constraint F; hence z_i is measured from this node line.

$$y_i = x_i\psi - z_i\gamma = x_i\psi - Rz_i\beta \tag{4}$$

$$\dot{y}_i = x_i\dot{\psi} - Rz_i\dot{\beta} \tag{5}$$

The lateral velocity $\dot{y}_i$ is the time derivative of Equation 4. Since x_i and y_i are nearly constant, $\dot{x}_i = \dot{z}_i = 0$. The total kinetic energy T and its derivatives are used to obtain the inertia moments of the surfaces.

$$T = \frac{1}{2}\sum_i m_i\left[x_i\dot{\psi} - Rz_i\dot{\beta}\right]^2$$

$$\left.\begin{aligned} \frac{d}{dt}\left(\frac{\partial T}{\partial\dot{\psi}}\right) &= \sum_i m_i\left[x_i^2\ddot{\psi} - Rz_ix_i\ddot{\beta}\right]; \quad \frac{d}{dt}\left(\frac{\partial T}{\partial\dot{\beta}}\right) = \sum_i m_i\left[-Rx_iz_i\ddot{\psi} + R^2z_i^2\ddot{\beta}\right] \\ &= I_aR^2\ddot{\psi} - PR\ddot{\beta}\ ; \qquad\qquad = -PR\ddot{\psi} + I_nR^2\ddot{\beta} \end{aligned}\right\} \tag{6}$$

where $I_a = \sum_i m_i x_i^2$, $I_n = \sum_i m_i z_i^2$, $P = \sum_i m_i x_i z_i$ (cf. p 26)

The generalized force terms Q_k are represented by the aerodynamic moments about the airplane c.g., and the "pseudo-moments" about the bent node line. According to D'Alembert's principle, the force of constraint F does not enter into the dynamic equations of motion. Then

$$Q_k = \sum_i \left(X_i \frac{\partial x_i}{\partial q_k} + Y_i \frac{\partial y_i}{\partial q_k} + Z_i \frac{\partial z_i}{\partial q_k} \right) \doteq \sum_i Y_i \frac{\partial y_i}{\partial q_k}, \text{ Since } X_i = Z_i \doteq 0$$

The summation is made by considering (i) as chordwise strips of the airfoil of width Δz, and integrating over the span. Then the aerodynamic forces become

$$Y_i = \sum_i C_{L_\alpha} q c \Delta z \left[\left(\psi - \frac{x}{U} \dot{\psi} \right) + \tau \left(\beta - \frac{x_\beta}{U} \dot{\beta} \right) \right]$$

Since $\frac{\partial y_i}{\partial \psi} = x_i$, and $\frac{\partial y_i}{\partial \beta} = -R z_i$, the generalized forces are

$$\Sigma M_{cg}: \quad Q_\psi = L_\alpha \left\{ \left(\psi - \frac{x}{U} \dot{\psi} \right) x + \tau \left(\beta - \frac{x_\beta}{U} \dot{\beta} \right) x \right\} \tag{7a}$$

$$\Sigma \text{"}M\text{"}_{node}: \quad Q_\beta = L_\alpha \left\{ \left(\psi - \frac{x}{U} \dot{\psi} \right)(-R z_\alpha) + \tau \left(\beta - \frac{x_\beta}{U} \dot{\beta} \right)(-R z_\beta) \right\} \tag{7b}$$

The equations of motion from Equations (6) and (7) are then as follows:

Moment due to	$\ddot{\psi}$	$\dot{\psi}$	ψ	$\ddot{\beta}$	$\dot{\beta}$	β	
about c.g. $\Sigma M_{cg} = 0$	$I_\alpha \ddot{\psi}$	$+L_\alpha \frac{x^2}{U} \dot{\psi}$	$-L_\alpha x \psi$	$-PR\ddot{\beta}$	$+L_\alpha \tau \frac{x x_\beta}{U} \dot{\beta}$	$-L_\alpha \tau x_\beta \beta$	$= 0$ (8a)
about node $\Sigma \text{"}M\text{"}_{node} = 0$	$-PR\ddot{\psi}$	$-L_\alpha \frac{R x z_\alpha}{U} \dot{\psi}$	$+L_\alpha R z_\alpha \psi$	$+I_n R^2 \ddot{\beta}$	$-L_\alpha \frac{\tau R x_\beta z_\beta}{U} \dot{\beta}$	$+L_\alpha \tau R z_\beta \beta$	$= 0$ (8b)

In these equations $x_\alpha, x_\beta, x, z, z_\alpha < 0 < L_\alpha, z_\beta$. The signs which precede each term then give the proper sense to the individual moment terms, according to the equation $\Sigma M = I\ddot{\theta} - \Sigma F \cdot l = 0$. Introducing the operator $\lambda = d/dt$, and dividing each equation by $I_\alpha = k m x^2$, the equations of motion then becoms

$$\left[\lambda^2+\frac{C_{L_\alpha}}{k}\left(\frac{\rho SU}{2m}\right)\frac{x^2}{x^2}\lambda-\frac{C_{L_\alpha}}{k}\left(\frac{\rho US}{2m}\right)\frac{xU}{x^2}\right]\psi+$$

$$+\left[-\frac{P}{I_a}R\lambda^2+\frac{C_{L_\alpha}\tau}{k}\left(\frac{\rho US}{2m}\right)\frac{xx_\beta}{x^2}\lambda-\frac{C_{L_\alpha}\tau}{k}\left(\frac{\rho US}{2m}\right)\frac{xU}{x^2}\right]\beta=0$$

$$\left[-\frac{PR}{I_a}\lambda^2-\frac{C_{L_\alpha}R}{k}\left(\frac{\rho US}{2m}\right)\frac{xz_\alpha}{x^2}\lambda+\frac{C_{L_\alpha}R}{k}\left(\frac{\rho SU}{2m}\right)\frac{z_\alpha U}{x^2}\right]\psi+$$

$$+\left[\frac{I_n}{I_a}R^2\lambda^2-\frac{C_{L_\alpha}\tau R}{k}\left(\frac{\rho US}{2m}\right)\frac{x_\beta z_\beta}{x^2}\lambda+\frac{C_{L_\alpha}\tau R}{k}\left(\frac{\rho US}{2m}\right)\frac{z_\beta U}{x^2}\right]\beta=0$$

The equations may then be reduced to dimensionless form by multiplying through by $\tau^2=\left(\frac{2m}{\rho US}\right)^2$, τ being the time factor. In this way

$\lambda^2\tau^2=\frac{d^2}{dt^2}$, $\lambda\tau=\frac{d}{dt}\tau$ become dimensionless.

$\lambda^2\tau^2=\lambda'^2$, $\lambda\tau=\lambda'$

The prime denotes the dimensionless form of the operator $\frac{d}{dt}$.

The dimensionless equations of motion become

$$\left[\lambda'^2+\frac{C_{L_\alpha}}{k}\lambda'-\frac{C_{L_\alpha}\mu}{k}\right]\psi=-\left[-\frac{P}{I_a}R\lambda'^2+\frac{C_{L_\alpha}\tau}{k}\frac{x_\beta}{x}\lambda'-\frac{C_{L_\alpha}\tau\mu}{k}\right]\beta$$

$$\left[-\frac{PR}{I_a}\lambda'^2-\lambda'\frac{C_{L_\alpha}R}{k}\frac{z_\alpha}{x}+\frac{C_{L_\alpha}R\mu z_\alpha}{k\ x}\right]\psi=-\left[\frac{I_n}{I_a}R^2\lambda'^2-\frac{C_{L_\alpha}\tau R}{k}\frac{x_\beta z_\beta}{x^2}\lambda'+\frac{C_{L_\alpha}\tau R\mu}{k}\frac{z_\beta}{x}\right]\beta$$

where μ denotes the dimensionless size factor $\frac{2m}{\rho Sx}=\frac{\tau U}{x}=\mu<0$

Take the quotient of the above equations, represent each term in abbreviated form, and drop the prime hereafter.

$$\frac{(a_2\lambda^2+a_1\lambda+a_0)\psi}{(c_2\lambda^2+c_1\lambda+c_0)\psi}=\frac{(b^2\lambda^2+b_1\lambda+b_0)\beta}{(d^2\lambda^2+d_1\lambda+d_0)\beta} \qquad (9)$$

Equation (9) expands into a quartic in λ

The quartic equation in λ is

$$
\begin{aligned}
&A\lambda^4+B\lambda^3+C\lambda^2+D\lambda+E=0\\
&(a_2d_2 - b_2c_2)\lambda^4\\
&+(a_2d_1+a_1d_2-b_2c_1-b_1c_2)\lambda^3\\
&+(a_2d_0+a_0d_2+b_2c_0-b_0c_2+a_1d_1-b_1c_1)\lambda^2\\
&+(a_1d_0+a_0d_1-b_1c_0-b_0c_1)\lambda\\
&+(a_0d_0 - b_0c_0)=0
\end{aligned}
\tag{10}
$$

The quartic factors into two quadratics

$$
\left[\lambda^2+\frac{B}{A}\lambda+\frac{C}{A}\right]\left[\lambda^2+\frac{D}{C}\lambda+\frac{E}{C}\right]=0 \tag{11}
$$

providing $|\lambda_{1,2}| >> |\lambda_{3,4}|$ which will soon be confirmed (of Eq. 17).

Solving for the coefficients of the quartic equation

$$
\left.
\begin{aligned}
A&=\frac{I_n}{I_a}R^2-\left(\frac{PR}{I_a}\right)^2=R^2\left[\frac{I_nI_a-P^2}{I_a^2}\right]\\
B&=\frac{C_{L_\alpha}R}{k}\left[\tau\frac{x_\beta}{x}\left(\frac{P}{I_a}-\frac{z_\beta}{x}\right)+R\left(\frac{I_n}{I_a}-\frac{z_\alpha P}{x I_a}\right)\right]\\
C&=\frac{C_{L_\alpha}R|\mu|}{k}\left[\tau\left(\frac{P}{I_a}-\frac{z_\beta}{x}\right)+R\left(\frac{I_n}{I_a}-\frac{P}{I_a}\right)\right]+\left(\frac{C_{L_\alpha}}{k}\right)^2\tau R\frac{x_\beta}{x}\left(\frac{z_\alpha-z_\beta}{x}\right)\\
D&=\left(\frac{C_{L_\alpha}}{k}\right)^2\tau R|\mu|\left[\frac{z_\alpha-z_\beta}{x}+\frac{x_\beta}{x}\left(\frac{z_\alpha-z_\beta}{x}\right)\right]\\
E&=\left(\frac{C_{L_\alpha}}{k}\right)^2\tau R\mu^2\left[\frac{z_\alpha-z_\beta}{x}\right]
\end{aligned}
\right\} \tag{12}
$$

The orders of magnitude of various terms in the above equations are as follows:

$$
\begin{aligned}
&\mathcal{O}(1)\sim C_{L_\alpha},\tau,k,\mu\\
&\mathcal{O}(.1)\sim R\\
&\mathcal{O}(.03)\sim \frac{x_\beta}{x},\frac{z_\beta}{x},\frac{z_\alpha}{x}\\
&\mathcal{O}(<.01)\sim \left(\frac{I_n}{I_a}-\frac{P^2}{I_a^2}\right);
\end{aligned}
$$

Note: $\left(\frac{P}{I_a}\right)^2$ may be varied from 0 to equivalent to I_n/I_a by proper mass balancing of the surfaces

Retaining only terms of greatest value, the quartic coefficients are

$$\left.\begin{aligned} A &= R^2\left[\frac{I_n}{I_a}-\frac{P^2}{I_a^2}\right] &&= R^2\{I\} \\ B &= \frac{C_{L_\alpha}\tau R}{k}\frac{x_\beta}{x}\left[\frac{P}{I_a}-\frac{z_\beta}{x}\right] &&= L\tau R\frac{x_\beta}{x}\{J\} \\ C &= \frac{C_{L_\alpha}\tau R}{k}|\mu|\left[\frac{P}{I_a}-\frac{z_\beta}{x}\right] &&= L\tau R|\mu|\{J\} \\ D &= \left(\frac{C_{L_\alpha}}{k}\right)^2\tau R|\mu|\left[\frac{z_\alpha-z_\beta}{x}\right] &&= L^2\tau R|\mu|\{K\} \\ E &= \left(\frac{C_{L_\alpha}}{k}\right)^2\tau R\mu^2\left[\frac{z_\alpha-z_\beta}{x}\right] &&= L^2\tau R\mu^2\{K\} \end{aligned}\right\} \quad (13)$$

The ratios of coefficients then become (14)

$$\frac{B}{A}=\left[\frac{C_{L_\alpha}\tau R}{k}\frac{I_a^2}{R^2(I_nI_a-P^2)}\right]\frac{x_\beta}{x}\left(\frac{P}{I_a}-\frac{z_\beta}{x}\right)=L\frac{\tau}{RI}\frac{x_\beta}{x}\{J\}$$

$$\frac{C}{A}=\left[\quad\text{"}\quad\right]|\mu|\left(\frac{P}{I_a}-\frac{z_\beta}{x}\right)=L\frac{\tau}{RI}|\mu|\{J\}$$

$$\frac{D}{A}=\left[\quad\text{"}\quad\right]\frac{C_{L_\alpha}}{k}|\mu|\left(\frac{z_\alpha-z_\beta}{x}\right)=L^2\frac{\tau}{RI}|\mu|\{K\}$$

$$\frac{E}{A}=\left[\quad\text{"}\quad\right]\frac{C_{L_\alpha}}{k}\mu^2\left(\frac{z_\alpha-z_\beta}{x}\right)=L^2\frac{\tau}{RI}\mu^2\{K\}$$

$$\frac{D}{C}=\frac{C_{L_\alpha}}{k}\frac{(z_\alpha-z_\beta)/x}{\left(\frac{P}{I_a}-\frac{z_\beta}{x}\right)}=L\left\{\frac{K}{J}\right\}$$

$$\frac{E}{C}=\frac{C_{L_\alpha}}{k}|\mu|\frac{(z_\alpha-z_\beta)/x}{\left(\frac{P}{I_a}-\frac{z_\beta}{x}\right)}=L|\mu|\left\{\frac{K}{J}\right\}$$

Dynamic Stability Criteria. The quartic Eq (10) represents stable motion providing

$$\frac{B}{A},\ \frac{C}{A},\ \frac{D}{A},\ \frac{E}{A}>0$$

and $$Q=\frac{BCD}{A^3}-\frac{D^2}{A^2}-\frac{B^2E}{A^3}>0 \quad (15)$$

Investigating the sense and magnitude of the various terms, the bracketted term $\left[\frac{C_{L_\alpha}\tau R}{k}\frac{I_a^2}{R^2(I_nI_a-P^2)}\right]>0$, if $\frac{I_n}{I_a}>\left(\frac{P}{I_a}\right)^2$ which may be assured by proper balancing of the surfaces.

$\frac{B}{A},\frac{C}{A},\frac{D}{A},\frac{E}{A}>0$

If $\frac{x_\beta}{x}, -\frac{z_\beta}{x}, \frac{z_\alpha}{x}, |\mu|, C_{L_\alpha}, R>0$, then all the ratios are positive, and

Routh's discriminant is found to be

$$\mathcal{R} = \left[\frac{\left(\frac{C_{L_\alpha}}{k}\right)^4\left(\frac{\tau}{R}\right)^3\mu^2}{\left\{\frac{I_n}{I_a}-\left(\frac{P}{I_a}\right)^2\right\}^3}\right]\left[\frac{\chi_\beta}{\chi}\left(\frac{P}{I_a}-\frac{z_\beta}{\chi}\right)^2\left(\frac{z_\alpha-z_\beta}{\chi}\right)-\frac{R}{\tau}\left(\frac{I_n}{I_a}-\frac{P^2}{I_a^2}\right)\left(\frac{z_\alpha-z_\beta}{\chi}\right)^2-\right.$$
$$\left.-\left(\frac{\chi_\beta}{\chi}\right)^2\left(\frac{P}{I_a}-\frac{z_\beta}{\chi}\right)^2\left(\frac{z_\alpha-z_\beta}{\chi}\right)\right] > 0$$
$$=\left[\frac{\left(\frac{C_{L_\alpha}}{k}\right)^4\left(\frac{\tau}{R}\right)^3\mu^2}{\left\{\frac{I_n}{I_a}-\left(\frac{P}{I_a}\right)^2\right\}^3}\right]\left[\frac{\chi_\beta}{\chi}\left(\frac{P}{I_a}-\frac{z_\beta}{\chi}\right)^2\left(\frac{z_\alpha-z_\beta}{\chi}\right)\right]\left[1-\frac{\chi_\beta}{\chi}-\frac{\frac{R}{\tau}\left(\frac{I_n}{I_a}-\frac{P^2}{I_a^2}\right)\left(\frac{z_\alpha-z_\beta}{\chi}\right)}{\frac{\chi_\beta}{\chi}\left(\frac{P}{I_a}-\frac{z_\beta}{\chi}\right)^2}\right] > 0 \qquad (16)$$

Using the sense and order of magnitude data (pp 20, 21), it is found that all the above brackets are positive, or may be so by proper mass balancing of the surfaces, to give a small value to $\frac{I_n}{I_a}-\left(\frac{P}{I_a}\right)^2$. Hence, complete stability exists, since $\mathcal{R} > 0$.

Factoring the quartic. The quartic equation may be factored into two quadratics (of Eq 11), providing $|\lambda_{1,2}| \gg |\lambda_{3,4}|$

$$\left.\begin{aligned}
|\lambda_{1,2}| &= \left|-\frac{B}{2A}\pm\sqrt{\left(\frac{B}{2A}\right)^2-\frac{C}{A}}\right| \doteq \sqrt{\frac{C}{A}} = \sqrt{\frac{C_{L_\alpha}\tau R}{kR^2(I_nI_a-P^2)}\cdot\frac{I_a^2|\mu|}{}\left(\frac{P}{I_a}-\frac{z_\beta}{\chi}\right)} \\
|\lambda_{3,4}| &= \left|-\frac{D}{2C}\pm\sqrt{\left(\frac{D}{2C}\right)^2-\frac{E}{C}}\right| \doteq \sqrt{\frac{E}{C}} = \sqrt{\frac{C_{L_\alpha}}{k}|\mu|\,\frac{(z_\alpha-z_\beta)/\chi}{\left(\frac{P}{I_a}-\frac{z_\beta}{\chi}\right)}} \\
\frac{|\lambda_{1,2}|}{|\lambda_{3,4}|} &= \sqrt{\frac{\tau}{R}\,\frac{\left(\frac{P}{I_a}-\frac{z_\beta}{\chi}\right)^2}{\left(\frac{I_n}{I_a}-\frac{P^2}{I_a^2}\right)\left(\frac{z_\alpha-z_\beta}{\chi}\right)}} = \sqrt{\frac{C_{L_\alpha}}{k}|\mu|\,\eta_D} \geq 3
\end{aligned}\right\} \qquad (17)$$

Since the root $\lambda_{1,2}$ is greater than three times the magnitude of $\lambda_{3,4}$, the quadratic factors are therefore a good approximation to the quartic equation. Both of the quadratics represent oscillatory modes of motion, as indicated by the fact that $\frac{C}{A} > \left(\frac{B}{2A}\right)^2$ and $\frac{E}{C} > \left(\frac{D}{2C}\right)^2$. These modes will henceforth be called the short-period and long-period modes, respectively.

Comparison with fixed control stability. The frequency and damping characteristics of the coupled tail may now be compared with those of a fixed tail of the same area (cf Table I). It will be noted that both modes of the coupled tail have greater damping and higher frequency than the fixed tail, the degree of improvement depending upon the proper adjustment of the various terms comprising I, J, K (cf Eq. 13).

Optimum proportions for dynamic stability. The stability criteria (cf Eqs. 15, 16) may now be considered with the purpose of obtaining a high value of effectiveness from the coupled tail. It is recalled that $P<0$ is necessary in order that angular acceleration $+\ddot{\psi}$ will give corrective control (cf pp 15, 16). However, the magnitude of $\frac{P}{I_a}$ must be less than $-\frac{z_\beta}{x}$, in order that the term $J = \frac{P}{I_a} - \frac{z_\beta}{x} > 0$, because $\frac{B}{A}, \frac{C}{A} > 0$, depend upon this condition (cf Eqs. 14). The term J should be made as small as practical, in order that $\frac{E}{C} = L|\mu| \frac{K}{J}$ should be large, since $\frac{K}{J}$ determine the period and damping of the long mode. The term $K = (z_\alpha - z_\beta)/x$ involves the centroid positions, which have been discussed at some length under static stability. It is noted that if P = o, then $\frac{K}{J} = (z_\beta - z_\alpha)/z_\beta = \eta_s$, the tail efficiency factor (cf Eq. 2).

In the adjustment of the mass balance of the coupled tail, the inertia term $I = \frac{I_n}{I_a} - \frac{P^2}{I_a^2} > 0$ requires that the product of inertia P should not be excessive. However in Routh's discriminant, (cf Eq. 16), the magnitude of the last term requires a proper value of P in the numerator and denominator. If P = o, the order of magnitude of the last term is $\Theta(\frac{1}{4})$ thus permitting considerable freedom of adjustment to get optimum proportions for high stability.

The final tests for stability are found to be as follows:

$$\eta_s, I, J, K > 0 \; ; \quad P \leq 0$$

Table I

Coupled Tail vs Fixed Tail

	Fixed Tail	Coupled Tail	
		Short-Period Mode	Long-Period Mode
Equation of motion (non-dimensional)	$\lambda^2 + L\lambda + L\mu = 0$	$\lambda^2 + \frac{B}{A}\lambda + \frac{C}{A} = 0$	$\lambda^2 + \frac{D}{C}\lambda + \frac{E}{C} = 0$
Damping ratio ξ	$\frac{L}{2\sqrt{L\mu}} = \frac{1}{2}\sqrt{\frac{L}{\mu}}$	$\frac{B}{2A}\sqrt{\frac{A}{C}} = \frac{1}{2}\frac{X_\beta}{X}\sqrt{\frac{L}{\mu}}\sqrt{\frac{\tau J}{RI}}$	$\frac{D}{2C}\sqrt{\frac{C}{E}} = \frac{1}{2}\sqrt{\frac{L}{\mu}}\sqrt{\frac{K}{J}}$
Undamped natural frequency ω_0	$\sqrt{L\mu}$	$\sqrt{\frac{C}{A}} = \sqrt{\frac{L}{\mu}\frac{\tau}{IR}J}$	$\sqrt{\frac{E}{C}} = \sqrt{L\mu}\frac{K}{J}$
Ratio $\frac{\xi \text{ coupled}}{\xi \text{ fixed}}$		$\frac{X_A}{X}\sqrt{\frac{\tau}{R}\frac{J}{I}}$	$\sqrt{\eta_D} = \sqrt{\frac{K}{J}} \doteq \sqrt{\eta_S}$ *
Ratio $\frac{\omega_0 \text{ coupled}}{\omega_0 \text{ fixed}}$		$\sqrt{\frac{\tau J}{RI}}$	$\sqrt{\eta_D} = \sqrt{\frac{K}{J}} \doteq \sqrt{\eta_S}$
Ratio $\frac{\xi \text{ short mode}}{\xi \text{ long mode}}$		$\frac{X_\beta}{X}\sqrt{\frac{\tau}{R}\frac{J^2}{IK}} = \Theta\left(\frac{1}{5}\right)$	
Ratio $\frac{\omega_0 \text{ short mode}}{\omega_0 \text{ long mode}}$		$\sqrt{\frac{\tau}{R}\frac{J^2}{IK}} = \Theta(5)$	
Ratio of time to damp to 1/2 amplitude	$\frac{\text{short mode}}{\text{long mode}} = \frac{D/2C}{B/2A} = \frac{1}{\frac{X_\beta}{X}\frac{\tau J^2}{RIK}} = \Theta\left(\frac{1}{2}\right)$		
Ratio of time to damp to 1/2 amplitude	$\frac{\text{long mode}}{\text{fixed tail}} = \frac{L/2}{D/2C} = \sqrt{\frac{J}{K}} \doteq \frac{1}{\sqrt{\eta_S}}$		

* $\eta_D = \frac{K}{J} = \frac{(z_\alpha - z_\beta)/x}{\left(\frac{P}{I_a} - \frac{z_\beta}{x}\right)}$; If $P \doteq 0$, $\eta_D = \frac{z_\beta - z_\alpha}{z_\beta} = \eta_S$ (cf Eq. 2)

Flutter consideration of coupled tail. The unstable condition discussed in the dynamic stability investigation may be considered a type of flutter which may be avoided by the application of definite rules which have been given.

The phase-lag inherent in a self-induced vibrating system, by means of which the system extracts energy from the air stream to actuate itself, is completely reversed in the properly balanced coupled surface, which conducts energy into the air stream by opposing a displacement, and therefore inhibits flutter conditions. The damping reaction leads the displacement vector by about 1/4 cycle and consequently is an anticipatory control (cf. Sec. V-A). The inertia effect increases with the square of the frequency; as a result, the short-period mode is more heavily damped than the long mode (cf. Table I). This fact is illustrated by the results of a simple test on model CFR-8. The coupled surface was restrained at $\psi=0$ in the wind tunnel, and the rudder was deflected to an angle β_0 and then released. The damped sine curve (cf. Fig. 11) which describes its return to $\beta=0$ exhi-

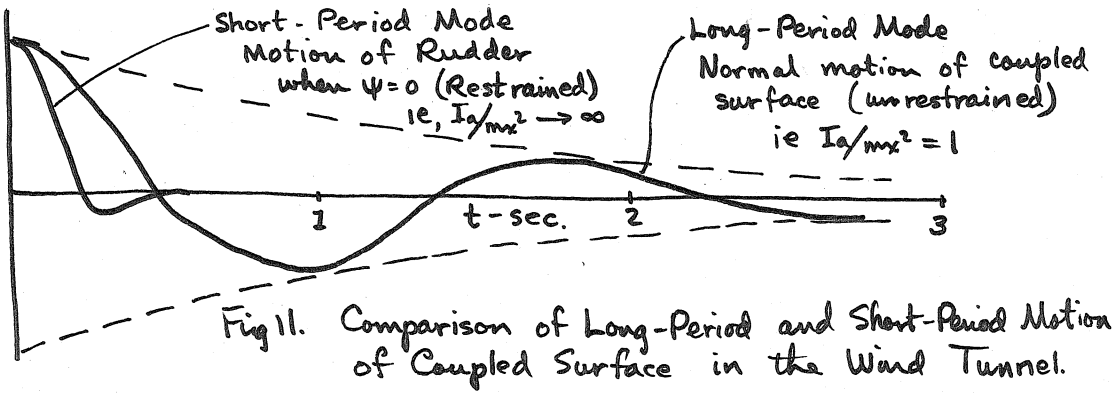

Fig 11. Comparison of Long-Period and Short-Period Motion of Coupled Surface in the Wind Tunnel.

bits a frequency of about 5 rad/sec and a damping ratio $\xi_{1,2} \doteq 0.5$, characteristic of the short-period mode with high I_z/mx^2. In contrast, when the surface was not restrained in yaw, the frequency was about π rad/sec for the long-period mode and the damping ratio $\xi_{3,4} \doteq 0.2$.

Consideration of Node Line. The position of the centroid of mass and the value of the "moment of intertia" I_n and "product of inertia" P with respect to the obtuse node line are more easily visualized by transforming the rudder contour to effect a straight node line at the base of the fin (cf. Fig. 12). The effects of coupling ratio R and mass distribution are then graphically illustrated.

It is noted that the product of inertia P may become positive for small values of R. The moment of inertia I_n about the node line likewise increases at small values of R.

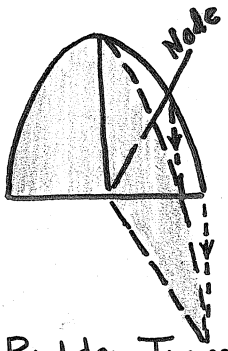

Fig. 12 Rudder Transformed to Give Straight Node Line

A new concept of importance to the static and dynamic stability theory is available through the transformation shown in Fig. 12.

The advantages to be derived from a more rearward x_β and a high c.g., as well as many other details for improving the coupled tail efficiency, may be seen by consideration of these relationships. The effect and magnitude of variations in some of the assumed-constant values may also be tested in this manner.

IV. Correlation of Theory with Tests

A. Description of Models and Tests

Two wind-tunnel models of the coupled tail were tested (cf. Table II and Ref. 7). The first of these (cf. Fig. 13) was made of mahogany and had a span of 11 inches and an area of 84 sq in. The second and larger model (cf. Fig. 14), made of aluminum alloy skin over a wooden framework of spars and ribs, had a span of 22 inches and an area of 2.64 sq ft. The airfoil sections were approximately NACA 0012, with rudder hinge at 50 per cent chord.

Table IV

Designations for Coupled Fin and Rudder Models

CFR No.	Description
1	Small wooden model (cf. Fig. 13) of vertical tail with end plate
2	Large sheet-metal model (cf. Fig. 14) of vertical tail with horizontal end plate, convex rudder surfaces, rounded and pinched trailing edge
3	Modification of No. 2, flat-sided rudder
4	Modification of No. 3, trailing edge square, plasticine added to make sides parallel to chord and extended aft even with edge of joggled trailing edge
5	Modification of No. 4, straight side of rudder faired into fin
6	Modification of No. 5, plasticine removed from trailing edge, giving a flat-sided rudder, faired into the fin, with joggled trailing edge
7	Modification of No. 6, 1/16 alclad plates extended to rear and lapped over external rudder surface at trailing edge, giving the rudder a concave side with a square trailing edge 1/4 thicker than that of No. 6
8	Same as No. 1 with modified planform, concave cambered trailing edge, symmetrical hinges, and coupling incorporated

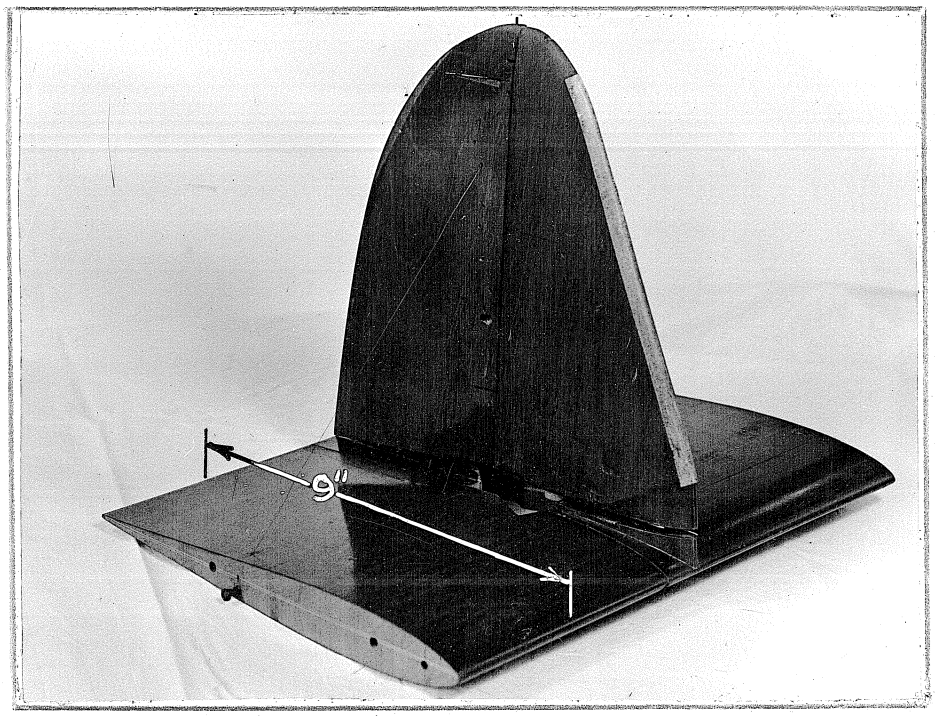

Fig. 13 Small Wind Tunnel Model CFR-1

Fig. 14 Large Wind Tunnel Model and Swinging Arm

The rudder surfaces were made flat in accordance with the normal practice for aircraft controls. These surfaces were first tested statically, to determine hinge-moment characteristics for predicting the maximum rearward position of the node line and the expected tail efficiency. Next they were tested as free-control coupled surfaces mounted on a swinging arm in the wind tunnel. The coupling was made by use of wire connected to the horizontal end plate, the attachment of the wire being adjustable on the rudder in order to change the node line to various positions. A more detailed description of the tests is given in Appendix D.

B. Results of Model Test Correlation

Excellent agreement was obtained between the static stability theory and wind tunnel test results with both models (cf. App. D). Dynamic stability tests were then made on the swinging arm in the wind tunnel. Of the nine cases which were studied, the final stability criteria gave the correct indication in every case. Four out of the nine configurations were stable. These encouraging results seem to indicate that the foregoing stability theory is a correct procedure to use in the design of coupled surfaces.

V. Effect of Coupled Surfaces on Airplane Stability

The thesis has already been proved that control surfaces coupled together as described provide much more powerful stability and damping than do fixed surfaces of equal area. This fact has been shown for the following cases:

1. As a wind vane, where only the tail inertia was involved, without the rest of the airplane.
2. As a wind vane having the normal mass and moment of inertia of an airplane, but with only the tail exerting aerodynamic forces.

It seems evident that the satisfactory behavior of the coupled surface as a wind vane proves that its use will be beneficial as an airplane stabilizer, since the many other aerodynamic effects will merely augment or diminish the large stability effect created by the tail. However, this hypothesis needs to be proved by reference to the general behavior of a real airplane and finally confirmed by the addition of the new characteristics to the equations of motion, which may then be solved for modes and stability criteria.

A. General Servo Mechanism Considerations

The purpose of a stabilizing surface on an airplane is to restore equilibrium conditions following a disturbance in a minimum of time and without perceptible oscillations. The motion following a disturbance of a one-degree-of-freedom vibrating system represented by the equation

$$a\ddot{\psi} + b\dot{\psi} + c\psi = 0 \text{ is}$$

$$\psi/\psi_0 = e^{-\xi\omega_0 t}\cos\omega_0 t = e^{-t/\tau}\cos\left(\frac{1}{\xi}\right)\frac{t}{\tau} \qquad (18)$$

where $\tau = 2a/b$ represents a characteristic time (cf. Refs. 8 and 9), $\xi = \frac{b}{2a\omega_o}$ the critical damping ratio as discussed in Section III-B, and $\omega_o = \sqrt{c/a}$ represents the undamped natural frequency of the coupled tail, when operating on its own moment of inertia, m x^2 only, as analyzed in Section III-B. The coupled tail was found to have two modes of motion, represented by short-period and long-period oscillations following a disturbance (cf. Table I).

Ratio of natural frequencies $\frac{\omega_o \text{ short mode}}{\omega_o \text{ long mode}} = \Theta\left(\frac{3}{1}\sqrt{\frac{c}{mx^2}}\right)$

Ratio of times to damp to 1/2 amplitude $\frac{\xi \text{short mode}}{\xi \text{long mode}} = \Theta\left(\frac{1}{10}\sqrt{\frac{c}{mx^2}}\right)$

Each of these modes will respond to a disturbance in accordance with Eq. 18, as shown in Fig. 15, where ξ = 0.2. A more desirable response to a disturbance is the nearly-aperiodic curve ξ = 0.5. Such a high degree of damping is not possible for ordinary stabilizing surfaces, but might be attained with a coupled tail having a tail efficiency of about 1.5, if such could be accomplished.

The ratio of relative amplitudes of the long and short modes following a static displacement was found by numerical solutions to be approximately as the ratio of the frequencies and independent of the forward velocity. These characteristics are believed to hold true in general

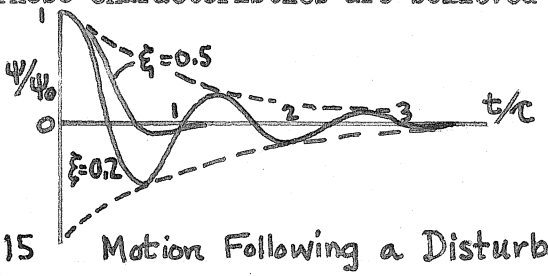

Fig.15 Motion Following a Disturbance

because of the relative magnitude of terms resulting from optimum proportions for dynamic stability (cf. Section III-B), which insures that the frequency separation of the modes shall be great and that both modes

shall have adequate damping. This procedure causes the short mode to vanish quickly, leaving the long mode predominant. Conversely, since the long mode is predominant, the procedure was correctly stated to increase the damping and natural frequency of the coupled tail and to insure that the long mode should predominate.

The damping ratio ξ for the long mode (cf. Table I) is

$$\xi = \frac{1}{2}\sqrt{\frac{C_{L\alpha}\frac{\rho}{2}U^2 S|x|}{(U^2/\chi^2)\,m\chi^2}}\;\sqrt{\frac{N}{I^\circ K}} = \frac{1}{2}\sqrt{\frac{C_{L\alpha}\frac{\rho}{2}S|x|}{m}}\sqrt{\eta_s}$$

The damping ratio is seen to be independent of the velocity. The natural frequency, however, increases linearly with the velocity.*

$$\omega_o = \sqrt{\frac{C_{L\alpha}\frac{\rho}{2}U^2 S|x|}{m\chi^2}}\sqrt{\eta_s}$$

If the coupled tail is operated as described (i.e., without the remainder of the airplane) in an air stream of velocity U, and the rudder is subjected to a sinusoidal forcing function of frequency ω_f, the response of each mode is as shown in point A of Fig. 16. When the same tail is installed on an airplane, the natural frequencies ω_o of the two modes remain the same, but the natural frequency of the airplane becomes less than the long mode of the tail alone, because of increased inertia and other effects. The natural frequency of the airplane-plus-tail becomes the new forcing frequency ω_f for the tail; as this frequency decreases with respect to the lowest ω_o of the tail alone, the ratio ω_f/ω_o decreases and the rudder action varies as shown in Fig. 16. The true stabilizing effect, measured by

---

* At altitude, both ξ and ω_o diminish with $\rho^{1/2}$, and both are augmented by $\eta_s^{1/2}$, thus providing an advantage over fixed surfaces.

the time to damp to 1/2 amplitude, then corresponds to point B, between the value determined for the dynamic condition as in Section III-B and the static condition as in Section III-A, depending on the change

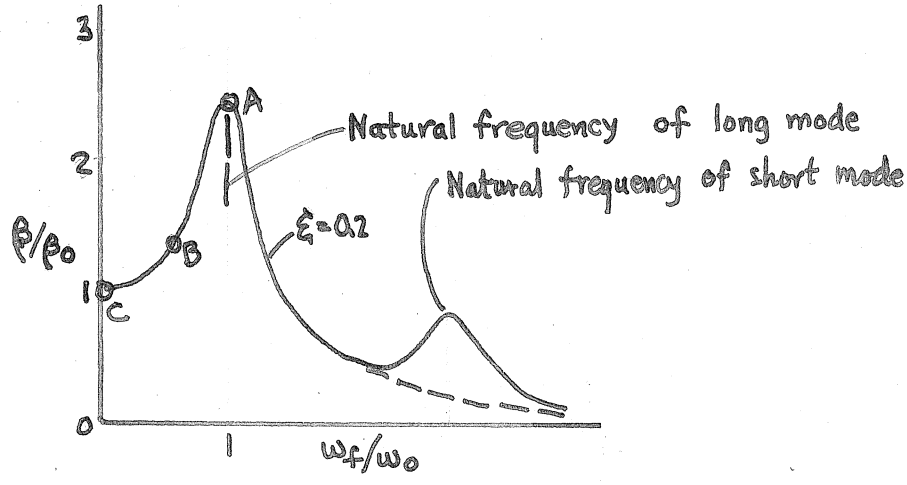

Fig.16 Response of Coupled Tail to Forced Oscillation

in frequency from tail alone to airplane-plus-tail. For extremely long-period motion, the static stability takes charge, and the improvement factor becomes $\eta_s = 1 + \tau_\beta / \psi$, corresponding to point C.

This qualitative discussion shows the general trend of the dynamic stability. However, in order to determine accurately the dynamic behavior of airplane-plus-tail, the equations of motion of the airplane, including the effect of the coupled tail, should be solved. The general solutions for longitudinal motion and lateral and directional motion will now be considered (cf. Ref. 10).

B. Lateral and Longitudinal Stability of Airplane

The complete force and moment equations for the airplane with respect to moving (Eulerian) axes are

$$X = m(\dot{u} - vr + wq)$$
$$Y = m(\dot{v} - wp + ur)$$
$$Z = m(\dot{w} - uq + vp)$$
$$L = A\dot{p} - (B-C)qr$$
$$M = B\dot{q} - (C-A)pr$$
$$N = C\dot{r} - (A-B)pq$$

Where the forces are X, Y, Z ; moments L, M, N ; moments of inertia A, B, C ; products of inertia D, E, F ; linear velocities u, v, w ; angular velocities p, q, r ; angular displacements Φ, θ, ψ ; all listed respectively to the coordinate axes x, y, z . The product of inertia $D, E, F = 0$, if axes are chosen to coincide with principal axes of the airplane. Dividing each equation by mass (or moment of inertia) gives the acceleration equations of motion.

$$\dot{u} = uX_u + wX_w + qX_q - g\theta\cos\theta_0$$
$$\dot{v} = vY_v + pY_p + rY_r + g\psi\sin\theta_0 + g\varphi\cos\theta_0 - U\dot{\psi}$$
$$\dot{w} = uZ_u + wZ_w + qZ_q - g\theta\sin\theta_0 + Uq$$
$$\dot{p} = vL_v + pL_p + rL_r$$
$$\dot{q} = uM_u + wM_w + qM_q$$
$$\dot{r} = vN_v + pN_p + rN_r$$

The modes of motion are separated in the conventional manner into longitudinal motion in the plane of symmetry, and lateral motion, which will be considered next.

Lateral stability. The lateral equations of motion for the airplane with coupled tail, each equation in terms of Force/Mass or Moment/MK^2 are

$$\left|\begin{array}{llll}
\hat{\lambda}=\frac{M}{\rho_1 SU} & (\lambda-Y_v)v + (-g\cos\theta_0)\varphi + (-g\sin\theta_0+U\lambda)\psi + (\text{Negl.}) & \beta = 0 \\
U\hat{\lambda}^2 & -L_v v + (\lambda^2-\lambda L_p)\varphi + (-L_r\lambda)\psi + (\text{Negl.}) & \beta = 0 \\
U\hat{\lambda}^2 & -N_v v + (-N_p)\varphi + (a_2\lambda^2+a_1\lambda)\psi + (b_2\lambda^2+b_1\lambda+b_0)\beta & = 0 \\
U\hat{\lambda}^2 & (\text{Negl.})v + (\text{Negl.})\varphi + (c_2\lambda^2+c_1\lambda+c_0)\psi + (d_2\lambda^2+d_1\lambda+d_0)\beta & = 0 \\
 & 1 \qquad \times\frac{1}{U} \qquad\qquad \times\frac{1}{U} \qquad\qquad \times\frac{1}{U} &
\end{array}\right\} \quad (19)$$

After performing the operations shown at the left and underneath Eqs. 19, the dimensionless equations are

$$F(\lambda) = \begin{vmatrix} \lambda-y_v & C_L & \lambda+C_L\theta_0 & \text{Negl.} \\ -\mu l_v & \lambda^2-\lambda l_p & -\lambda l_r & \text{Negl.} \\ -\mu n_v & -\lambda n_p & a_2\lambda^2+a_1\lambda & b_2\lambda^2+b_1\lambda+b_0 \\ \text{Negl.} & \text{Negl.} & c_2\lambda^2+c_1\lambda+c_0 & d_2\lambda^2+d_1\lambda+d_0 \end{vmatrix} = 0 \qquad (20)$$

where the coefficients a, b, c, d from the coupled tail dynamics (cf. Eqs. 8) have been reduced to dimensionless form in a manner similar to the airplane stability coefficients. The true sense of each term in the determinant $-F(\lambda)$ is as follows:

	v	φ	ψ	β
Y	− −	+	− +	Negl.
L	−	− −	+	Negl.
N	+	−	− − −	+ − −
H	−	Negl	+ + +	− − −

In these equations $C_{L_\alpha}, b/2, U$ are +; $C_L, C_{L_{dw}}, \alpha$ are −, and $\psi = -v/U$.

The non-dimensional determinant is next written in symbolic form and expanded.

$$F(\lambda) = \begin{vmatrix} y_v & y_\varphi & y_\psi & (y_\beta) \\ l_v & l_\varphi & l_\psi & (l_\beta) \\ (n_v) & n_\varphi & n_\psi & n_\beta \\ (h_v) & (h_\varphi) & h_\psi & h_\beta \end{vmatrix} = 0 = \sum_{i=0}^{n} A_i\lambda^i = h_\beta D - h_\psi n_\beta \begin{vmatrix} y_v & y_\varphi \\ l_v & l_\varphi \end{vmatrix}$$

The airplane stability with 3 degrees of freedom is represented by the 3 x 3 minor, and defined by D, whereas the coupled tail alone (cf. Eqs. 8) is given by the 2 x 2 minor. In the expansion, the terms n_ψ and h_v are transferred to $-n_{\dot{\beta}}y_v$ and $-h_\psi$ respectively, and terms h_φ, y_β and l_β are considered of negligible importance, thus creating zeros in the determinant and simplifying the expansion.

The evaluation of $h_\beta D$ is accomplished with the aid of the 3-dimensional equations of motion, whose determinant is $\mathbb{D}$.

$$h_\beta D = (d_2\lambda^2+d_1\lambda+d_0)\begin{vmatrix} \lambda-y_v & C_L & \lambda+C_L\theta_0 \\ -\mu l_v & \lambda^2-l_p\lambda & -l_r\lambda \\ -\mu n_v & -n_p\lambda & \lambda^2-n_r\lambda \end{vmatrix} = \sum_{i=0}^{n} A_i\lambda^i = f_1(\lambda)$$

The determinant $\mathbb{D}$ is expanded into a quintic equation in λ, of which one root is zero and may be discarded, thus leaving a quartic.

$$D = \begin{Bmatrix} \lambda^4 \\ +\lambda^3[-l_p-n_r-y_v] \\ +\lambda^2[\mu n_v+l_p n_r+(l_p+n_r)y_v-n_p l_r] \\ +\lambda\,[\mu n_v(C_L\theta_0-l_p)+\mu l_v(C_L+n_p)+y_v(n_p l_r-l_p n_r)] \\ +C_L[\mu(n_v l_r-l_v n_r)+\mu\theta_0(l_v n_p-n_v l_p)] \end{Bmatrix} \doteq \begin{Bmatrix} \lambda^4 \\ +\lambda^3[-n_v(\frac{\chi}{b/2}+\frac{l_p}{n_v})] \\ +\lambda^2[\mu n_v(1+\frac{l_p}{\mu}\frac{\chi}{b/2})] \\ +\lambda[-\mu n_v l_p] \\ +\mu n_v C_L[l_r-l_v\frac{\chi}{b/2}] \end{Bmatrix}$$

Next in order for evaluation is

$$-h_\psi n_\beta\begin{vmatrix} y_v & y_\varphi \\ l_v & l_\varphi \end{vmatrix} \doteq -(b_2\lambda^2+b_1\lambda+b_0)(c_2\lambda^2+c_1\lambda+c_0)\begin{vmatrix} \lambda-y_v & C_L \\ -\mu l_v & \lambda^2-l_p\lambda \end{vmatrix} = f_2(\lambda)$$

Terms $b_2 = c_2 \doteq 0$ for properly balanced surfaces, where z is small.

Then

$$f_2(\lambda) = (-)\begin{Bmatrix} \lambda^5[c_1b_1] \\ +\lambda^4[-c_1b_1(l_p+y_v)+(c_1b_0-c_0b_1)] \\ +\lambda^3[c_1b_1 l_p y_v-(c_1b_0+c_0b_1)(l_p+y_v)+c_0b_0] \\ +\lambda^2[(c_1b_0+c_0b_1)l_p y_v-c_0b_0(l_p+y_v)+c_1b_1\mu l_v C_L] \\ +\lambda[(c_1b_0+c_0b_1)\mu l_v C_L+c_0b_0 l_p y_v] \\ +[c_0b_0\mu l_v C_L] \end{Bmatrix} \doteq (-)\begin{Bmatrix} \lambda^5[c_1b_1] \\ +\lambda^4[c_1b_0+c_0b_1] \\ +\lambda^3[c_0b_0-(c_1b_0+c_0b_1)(l_p+y_v)] \\ +\lambda^2[-c_0b_0(l_p+y_v)] \\ +\lambda[c_0b_0 l_p y_v] \\ +[c_0b_0\mu l_v C_L] \end{Bmatrix}$$

The lateral stability derivatives (cf. Table III) may now be calculated for a conventional transport airplane (cf. Table IV).

Table III

Lateral Stability Derivatives

$l_p = \frac{1}{ka}\frac{dC_{l_w}}{d\alpha} = \frac{1}{3\times 0.05}(-4.3)$	-29
$l_r = -2C_L/ka = -2(-0.5)/3\times 0.05$	$+6.7$
$l_v = \frac{0.45}{a}\frac{T^0}{57.3}\frac{dC_{l_w}}{d\alpha} = \frac{0.45}{0.05}\frac{1}{57.3}(-4.3)$	-0.67
$\mu l_v = 27(-0.67)$	-18
$n_p = -\frac{1}{KC}\frac{dC_x}{d\Delta\alpha} = -\frac{1}{3\times 0.10}(+0.5)$	-1.67
$n_r = \frac{2C_D}{KC} - \frac{C_{L_\alpha}}{C}\frac{S_t}{S}\left(\frac{x}{b/2}\right)^2 \doteq -\frac{C_{L_\alpha}}{C}\frac{S_t}{S}\left(\frac{x}{b/2}\right)^2 = +n_v\frac{x}{b/2}$	-1.5
$n_v = -\frac{C_{L_\alpha}}{C}\frac{S_t}{S}\frac{x}{b/2} = -\frac{2}{0.10}\times 0.12(-.8)$	$+1.9$
$\mu n_v =$	$+50$
$y_r = -\frac{dC_y}{d\alpha}$	-0.50
$a_2 = (mx^2 + C')/MK_c^2 =$	$+1.0$
$b_2 = c_2 = -mR(xz)^+/MK_c^2 \doteq$	0
$d_2 = mR^2z^{2*}/MK_c^2 = 5\left(\frac{1}{8}\right)^2\frac{8^2}{10^6}$	5×10^{-6}
$a_1 = \frac{-L_\alpha x^2}{MK_c^2U}\frac{M}{\frac{\rho}{2}SU} = -\frac{C_{L_\alpha}}{C}\frac{S_t}{S}\left(\frac{x}{b/2}\right)^2 = -n_r$	$+1.5$
$b_1 = -n_r\tau x_\beta/x = 1.5\times 0.70/40$	0.0262
$c_1 = n_r R z_\alpha/x = -1.5\frac{1}{8}\frac{1}{80}$	-0.0023
$d_1 = n_r\tau R x_\beta z_\beta/x^2 = -1.5\times\frac{0.70}{8}\left(\frac{-1}{40}\right)^2$	$+0.000082$
$a_0 = \frac{-L_\alpha}{MK_c^2}\times\left(\frac{M}{\frac{\rho}{2}SU}\right)^2 = \left(-\frac{C_{L_\alpha}}{C}\frac{x}{b/2}\frac{S_t}{S}\right)\mu = \mu n_v$	$+50$
$b_0 = \mu n_v\tau = 50\times 0.70$	$+35$
$c_0 = -\mu n_v R z_\alpha/x = -\frac{50}{8}\frac{1}{80}$	-0.078
$d_0 = -\mu n_v\tau R z_\beta/x = -\frac{35}{8}\left(\frac{-1}{40}\right)$	$+0.110$
$b_1c_1 = -n_r^2\tau R x_\beta z_\alpha/x^2 = -(1.5)^2\frac{0.70}{8}\left(\frac{-1}{40}\right)\frac{1}{80}$	-0.000063
$b_0c_0 = -(\mu n_v)^2\tau R z_\alpha/x = -(50)^2\frac{0.70}{8}\frac{1}{80}$	-2.74
$b_0c_1 + b_1c_0 = 35(-.0023) + 0.0262(-.078)$	-0.083
$-n_v\left(\frac{x}{b/2} + \frac{l_p}{n_v}\right) = -1.9\left(-.8 + \frac{-29}{1.9}\right)$	$+30.6$
$\mu n_v\left(1 + \frac{l_p}{\mu}\frac{x}{b/2}\right) = 50\left(1 + \frac{-29\times 0.8}{27}\right)$	$+93$
$-\mu n_v l_p = -50(-29)$	$+1450$
$\mu n_v C_L\left(l_r - l_v\frac{x}{b/2}\right) = 50(0.5)\left(6.7 - (-0.67\times -0.8)\right)$	-155

Table IV

Data and Characteristics for Transport Airplane

Symbol	Item	Units	Value	Symbol	Item	Units	Value
W	Gross Weight	lbs	50,000	M	Airplane Mass	slugs	1600
S_w	Wing Area	sq ft	1,000	m	Tail Mass	slugs	5
S_t	Tail Area	sq ft	120	B = I_{yy}		slug ft^2	0.5×10^6
b	Wing Span	ft	100	C = I_{zz}		slug ft^2	10^6
χ	c.g.$_A$ to c.p. tail	ft	-40	$L_\alpha = C_{L_\alpha} q S_t$		lb/rad	24000
U	Airplane Velocity	mph	200	$\mathcal{T} = M/\frac{\rho}{2} S U$			3.5
q	Dynamic Pressure	$\frac{lbs}{sq\ ft}$	100	$\mu = M/\frac{\rho}{2} S \frac{b}{2}$			27
R	Coupling Ratio		0.125	z_α		ft	-0.5
$\tau = \frac{dC_L}{d\beta} / \frac{dC_L}{d\alpha}$			0.70	z_β		ft	1.0
χ_β		ft	-1.0	$\eta_S = \frac{z_\beta - z_\alpha}{z_\beta}$			1.5
$1 + \frac{r^2}{\chi^2}$			50	$\eta_D = \frac{z_\beta - z_\alpha}{z_{\beta^\circ}}$			0.03

It will be noted that a rather conservative value of the coupled tail efficiency is used, $\eta_S = 1.5$, in order to determine the beneficial effect of this moderate arrangement, in comparison with the conventional tail.

The lateral stability of the transport airplane with conventional tail is found by solving the determinant D (cf. Eq. 2b) which gives the frequency equation and factors as follows:

$$\lambda^4 + 30\lambda^3 + 93\lambda^2 + 1450\lambda - 155 = 0$$
$$(\lambda - 0.107)(\lambda + 28.5)(\lambda^2 + 1.5\lambda + 53) = 0$$

The conventional airplane will therefore have a spiral divergence which doubles in 45 sec, a roll subsidence, and oscillation in roll and yaw of

3 sec period and ξ = .10 times critical damping; i.e., damping to one-half amplitude in 3.2 sec.

The complete determinant $F(\lambda) = f_1(\lambda) + f_2(\lambda) = \Sigma A_i \lambda^i$ may now be evaluated to determine the behavior of the same airplane equipped with the coupled tail.

i	$h_\beta D$	$-h_\psi n_\beta \vert::\vert$	A_i
6	$d_2 = 5\times10^{-6}$		5×10^{-6}
5	$d_2[-n_v(\frac{x}{b/2} + \frac{l_p}{n_v})] + d_1[\ ] + d_0[\ ]$ [30] .000083	$-b_1c_1$ (-.000063)	0.00030
4	$d_2[\mu n_v(1+\frac{l_p}{\mu}\frac{x}{b/2})] + d_1[\ ] + d_0[\ ]$ [93] .108	$-(b_0c_1 + b_1c_0)$ (-.085)	0.193
3	$d_2[-\mu n_v l_p\ ] + d_1[\ ] + d_0[\ ]$ [1450] 3.2	$-b_0c_0 + (\ )(l_p + y_v)$ (-29)	8.5
2	$d_2[\mu n_v C_L(l_r - l_v\frac{x}{b/2})] + d_1[\ ] + d_0[\ ]$ [-155] 10	$b_0c_0(l_p + y_v)$ (-29)	91.
1	$d_1[\ ] + d_0[\ ]$ 156	$-b_0c_0\, l_p\, y_v$ (14.5)	196.
0	$+d_0[\ ]$ -17	$-b_0c_0\,\mu\, l_v\, C_L$ (18) (-.5)	8.

The frequency equation and its factors then become

$$\lambda^6 + 10^6[.000060\lambda^5 + 0.0386\lambda^4 + 1.70\lambda^3 + 18.2\lambda^2 + 39.2\lambda + 1.6] = 0$$

$$(\lambda + 14.4)(\lambda + 30)(\lambda^2 + 13\lambda + 37500)(\lambda + 2.34)(\lambda + 0.059) = 0$$

The lateral modes of the airplane with coupled tail are thus found to be two heavily damped aperiodic modes, one of which resembles the roll subsidence $(\lambda - l_p)$; a short period oscillation of 0.1 sec period which damps to ½ amplitude in 0.4 sec and for which ~~and~~ ξ = 0.03* times critical damping; and two more aperiodic modes which damp to one-half amplitude in 2 and 80 sec. resp.

A comparison of the effect of coupling on the lateral stability may now be made.

* Viscous damping could be used to increase ξ, if desired.

Mode	Characteristic	Conventional Tail	Coupled Tail
Spiral	Time to ——, sec	45 to Double	80 to Halve
Roll	Time to halve, sec	.16	.16
Oscillation	Period, sec	3.0	0.11
n	Fraction of Crit. Damping	0.105	0.03
N	Time to Halve, Sec	3.2	0.40

The normally divergent spiral mode, which is characteristic of a fixed control airplane with a powerful vertical tail, has been overcome and damped by the magnitude of the controlling moments introduced by the coupled tail. Likewise the conventional oscillation in roll and yaw of 3 sec period seems to have been eliminated, or replaced by an extremely short oscillation of 0.11 sec period, which damps to one-half amplitude in 0.40 sec. A worthwhile improvement in lateral stability is thus demonstrated for a transport airplane at cruising speed, equipped with a coupled tail having a moderate value of efficiency $\eta_s = 1.5$.

Longitudinal stability. The longitudinal equations of motion in terms of Force/M or Moment/MK^2 are

$$\begin{array}{c|cccc|c} & 1 & 1 & \frac{1}{U} & \frac{1}{U} & \\ \hline \hat{X} & (\lambda - X_u)u & -X_w w & +(g\cos\theta_0)\theta & +N_{eg}\beta & =0 \\ \hat{Z} & -Z_u u & +(\lambda - Z_w)w & +(g\sin\theta_0 - U\lambda)\theta & -Z_\beta\beta & =0 \\ U\hat{M}^2 & -M_u u & -M_w w & +(a_2\lambda^2+a_1\lambda+a_0)\theta & +(b_2\lambda^2+b_1\lambda+b_0)\beta & =0 \\ U\hat{N}^2 & N_{eg} & N_{eg} & +(c_2\lambda^2+c_1\lambda+c_0)\theta & +(d_2\lambda^2+d_1\lambda+d_0)\beta & =0 \end{array} \qquad (22)$$

After performing the necessary operations to convert the determinant of coefficients to non-dimensional form, the longitudinal equations of motion are

$$F(\lambda) = \begin{vmatrix} \lambda - x_u & -x_w & -c_L & 0 \\ -z_u & \lambda - z_w & -c_L\theta_0 - \lambda & -z_\beta \\ -\mu m_w & -\mu m_w & a_2\lambda^2 + a_1\lambda + a_0 & b_2\lambda^2 + b_1\lambda + b_0 \\ 0 & 0 & c_2\lambda^2 + c_1\lambda + c_0 & d_2\lambda^2 + d_1\lambda + d_0 \end{vmatrix} = 0 \qquad (22)$$

The true sense of each term in $-F(\lambda)$ is as follows:

	u	w	θ	β
X	− −	+	0	0
Z	−	− −	0	0
M	−	−	− − −	+ − −
H	0	+	+ + +	− − −

In these equations, the terms $C_L, C_{L_\alpha}, C_{L_{\alpha_w}}, \chi$ are considered −.

The non-dimensional determinant is next written in symbolic form and expanded, with the aid of the assumptions that x_β, z_β, m_u and h_u are negligible, a_0 is transferred to $-\mu m_w$, and h_w is transferred to c_0. Then

$$F(\lambda) = \begin{vmatrix} x_u & x_w & x_\theta & 0 \\ z_u & z_w & z_\theta & 0 \\ 0 & m_w & m_\theta & m_\beta \\ 0 & 0 & h_\theta & h_\beta \end{vmatrix} = h_\beta D - h_\theta m_\beta \begin{vmatrix} x_u & x_w \\ z_u & z_w \end{vmatrix} = \sum_i A_i \lambda^i = 0$$

$$= f_1(\lambda) + f_2(\lambda)$$

The evaluation of $h_\beta D$ is accomplished by use of the 3-dimensional equations of motion, whose determinant is D.

$$h_\beta D = (d_2\lambda^2 + d_1\lambda + d_0) \begin{vmatrix} \lambda - x_u & -x_w & -c_L \\ -z_u & \lambda - z_w & -c_L\theta_0 - \lambda \\ 0 & -\mu m_w & \lambda^2 - \lambda m_q \end{vmatrix} = f_1(\lambda)$$

$$= (d_2\lambda^2 + d_1\lambda + d_0)\left\{\lambda^4 + (-x_u - z_w - m_q)\lambda^3 + \left[(x_u z_w - z_u x_w) + (x_u + z_w)m_q - \mu m_w\right]\lambda^2 + \right.$$
$$\left. + \left[\mu m_w(x_u - c_L\theta_0) + m_q(z_u x_w - x_u z_w)\right]\lambda + \mu m_w c_L(x_u\theta_0 - z_u)\right\}$$

Next in order for evaluation is

$$-h_\theta m_\beta \begin{vmatrix} x_u & x_w \\ z_u & z_w \end{vmatrix} = -(b_2\lambda^2+b_1\lambda+b_0)(c_2\lambda^2+c_1\lambda+c_0)\begin{vmatrix} \lambda-x_u & -x_w \\ -z_u & \lambda-z_w \end{vmatrix} = f_2(\lambda)$$

where $b_2 = c_2 \doteq 0$ for properly balanced surfaces. Then

$$f_2(\lambda) = -\{b_1c_1\lambda^4+[(b_1c_0+b_0c_1)-b_1c_1(x_u+z_w)]\lambda^3+[b_0c_0+b_1c_1(x_uz_w-z_ux_w)-(b_1c_0+b_0c_1)(x_u+z_w)]\lambda^2+$$
$$+[(b_1c_0+b_0c_1)(x_uz_w-z_ux_w)-b_0c_0(x_u+z_w)]\lambda+b_0c_0(x_uz_w-z_ux_w)\}$$

The complete determinant $F(\lambda) = f_1+f_2 = \Sigma A_i\lambda^i$ may now be evaluated for a conventional transport airplane using data from Tables VIII and IX.

i	$h_\beta D$	$-h_\theta m_\beta \begin{vmatrix} \cdot & \cdot \\ \cdot & \cdot \end{vmatrix}$	A_i
6	$d_2 = 20\times10^{-6}$		20×10^{-6}
5	$d_2(-x_u-z_w-m_q)$ (9.0) $+ d_1$ .00033		0.00045
4	$d_2(z_wm_q-\mu m_w)$ (48) $+d_1[\ ]+d_0$ .079	$-b_1c_1$ (−.00054)	0.063
3	$d_2\begin{pmatrix}\mu m_w(x_u-c_1\theta_0)\\ m_q(z_ux_w-x_uz_w)\end{pmatrix}$ (62) $+d_1[\ ]+d_0[\ ]$ .53	$-(b_1c_0+b_0c_1)+b_1c_1(x_u+z_w)$ (−.137) (−4.9)	0.66
2	$d_2[\mu m_w c_1(x_u\theta_0-z_u)]$ [13.5] $+d_1[\ ]+d_0[\ ]$ 2.8	$-b_0c_0+[\ ][\ ]-$ (−.8) $-2b_1c_1(x_uz_w-z_ux_w)$ (.78)	3.0
1	$+d_1[\ ]+d_0[\ ]$ .36	$+[\ ][\ ]-[\ ][\ ]$ 7.0	3.9
0	$+d_0[\ ]$ .80	$-[\ ][\ ]$	1.0

Table IX

Longitudinal Stability Derivatives

$x_u = 2C_D = 2(-0.05)$	-0.10
$x_w = -C_{Lw} + C_{D_2} = -(-0.5)\left[1 + \frac{2}{10\pi}(-4.3)\right]$	$+0.35$
$z_u = 2C_{Lw} = 2(-0.5)$	-1.0
$z_w = C_{L_{dw}}$	-4.3
m_u	0
$m_w = \frac{1}{b}\left[C_{L_{dw}} \frac{c}{L}\left(\frac{a}{c} - k\right) + C_{L_{dt}} \frac{S_t}{S} e\left(1 - \frac{d\epsilon}{d\alpha}\right)\right]$	$\begin{cases} -1.0 \text{ Fixed} \\ -0.5 \text{ Coupled} \end{cases}$
$m_q = 1.2 C_{L_\alpha} \frac{S_t}{S} \frac{e}{b}\left[1 + Q(r-1)\right]$	-4.5
$\mu \frac{m_w}{m_q}$	6.0
$a_2 =$	1.0
$b_2 = c_2 = mR(xz)^+ / MK_B^2$	0
$d_2 = mR^2 z^{2*} / MK_B^2 = 8 \times \frac{80}{64} / .5\times10^6$	20×10^{-6}
$a_1 = \frac{-L_\alpha}{MK_B^2} \frac{\chi^2}{U} \frac{M}{\frac{\rho}{2} SU} = -\frac{C_{L_\alpha}}{b} \frac{S_t}{S} e = -m_q$	$+4.5$
$b_1 = -m_q \tau x_\beta / x = 4.5 \times \frac{0.70}{40}$	0.079
$c_1 = m_q R z_\alpha / x = -\frac{4.5}{8} \frac{1}{80}$	-0.0070
$d_1 = m_q \tau R x_\beta z_\beta / x^2 = -4.5 \frac{.70}{8} \frac{1}{40}\left(-\frac{1}{40}\right)$	$+0.00025$
$a_0 = \frac{L_\alpha}{MK_B^2} \frac{x}{\left(\frac{M}{\frac{\rho}{2}SU}\right)^2} = \frac{C_{L_\alpha}}{b} \frac{S_t}{S} \mu e = -\mu m_w$	$+27$
$b_0 = -\mu m_w \tau = 27 \times 0.7$	$+19$
$c_0 = \mu m_w R z_\alpha / x = -\frac{27}{8} \frac{1}{80}$	-0.042
$d_0 = \mu m_w \tau R z_\beta / x = -\frac{27}{8} \times 0.7 \times \left(-\frac{1}{40}\right)$	0.059
$b_0 c_0 = -(\mu m_w)^2 \tau R z_\alpha / x = -(27)^2 \frac{0.7}{8} \frac{1}{80}$	-0.80
$b_1 c_1 = -(m_q)^2 \tau R x_\beta z_\alpha / x^2 = -(4.5)^2 \frac{0.7}{8} \frac{1}{40} \frac{1}{80}$	-0.00054
$b_0 c_1 + b_1 c_0 = -\mu m_w m_q \tau R z_\alpha / x = -(-27)(-4.5) \frac{0.7}{8} \frac{1}{80}$	-0.137
$-x_u - z_w - m_q = 0.10 + 4.3 + 4.5$	8.9
$-\mu m_w + m_q(x_u + z_w) + (x_u z_w - z_u x_w) = -27 - 4.5(-4.4) + .8$	$+48.$
$\mu m_w (x_u - C_L \theta_0) + m_q (z_u x_w - x_u z_w) = -27(-.10) - 4.5(-.78)$	6.2
$\mu m_w C_L (x_u \theta_0 - z_u) = -27(-0.5)$	13.5

The longitudinal frequency equation and its factors are

$$\lambda^6 + 22\lambda^5 + 3150\lambda^4 + 33{,}000\lambda^3 + 150{,}000\lambda^2 + 195{,}000\lambda + 50{,}000 = 0$$

$$(\lambda + .34)(\lambda + 1.5)(\lambda^2 + 12\lambda + 2980)(\lambda^2 + 9\lambda + 33) = 0$$

The modes of motion are thus found to be two aperiodic modes and two well damped oscillations. The short-period oscillation, which is characteristic of the tail dynamics, has a period of 0.40 sec and $\xi = 0.11$ times critical damping; i.e., damp to one-half amplitude in 0.40 sec. The long-period motion has a period of 3.8 sec and $\xi = 0.78$ times critical damping; i.e., damp to one-half amplitude in 0.54 sec.

The stability of the same airplane with conventional controls may be determined for comparison.

$$\lambda^4 + 9\lambda^3 + 48\lambda^2 + 6.2\lambda + 13.5 = 0$$

$$(\lambda^2 + 9\lambda + 48)(\lambda^2 + 0.09\lambda + 0.28) = 0$$

The modes are a short period of 3.2 sec, $\xi = 0.65$, and a long period of 41 sec, $\xi = 0.085$. The two oscillations are now shown for comparison.

Mode	Characteristic	Conventional	Coupled
Short Period	Period, sec Fraction of Crit. Damping Time to Halve, Sec.	3.2 0.65	0.40 0.11 0.40
Long Period	Period, Sec. Fraction of Crit. Damping Time to Halve, Sec.	41 0.085 54	3.8 0.78 0.54

A considerable improvement has thus been effected in the longitudinal stability of the airplane. The poorly damped long-period oscillation is eliminated by use of the coupled tail, and the resulting short-period modes are sufficiently well damped that they will require no control; in

fact, they would hardly be recognized as oscillation by passengers in the airplane.

C. Effect of Friction

The theoretical stability analysis assumes no friction or free play in the control system. The original hypothesis is that rudder deflection β is proportional to yaw angle ψ at all times. However, when the friction hinge moment (F.H.M.) is greater than the aerodynamic hinge moment $\beta C_{H_\beta} q S_t c_r$, the surface will remain deflected to an angle β_F, until a larger aerodynamic hinge moment causes it to move, where $\beta_F = FHM / C_{H_\beta} q S_t c_r$
By definition of coupling ratio, $R = \beta_F / \psi_F$.

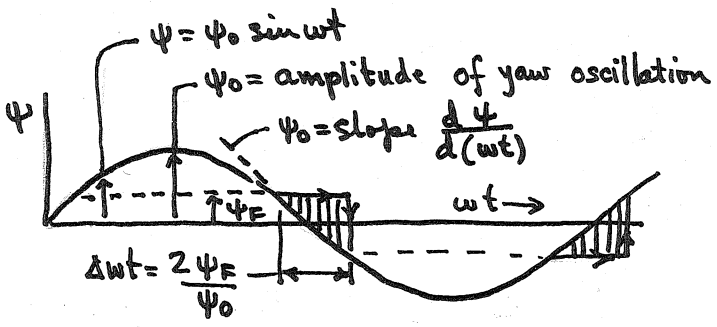

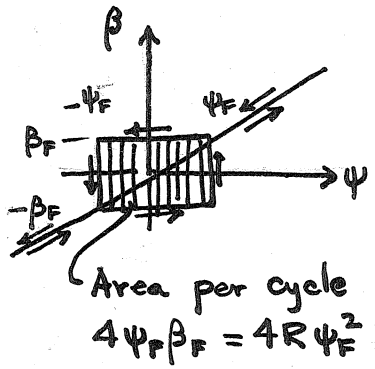

Consider the coupled surface to be oscillating with an initial amplitude ψ_0. Without friction, the oscillation would be damped to zero amplitude in a short time. With friction, the rudder sticks at β_F, corresponding to ψ_F, until the yaw angle reaches $-\psi_F$, after which the rudder jumps to the value of $-\beta_F$ and thenceforth is proportional to ψ until next crossing the $\pm\psi_F$ band. The control deflections corresponding to the sticky action are incorrect for damping the motion, and the energy per cycle extracted from the air stream due to the friction lag angle ψ_F is approximately

$$W_F = \eta C_{L_\alpha} q S_t l \left(4 \psi_F \beta_F\right) = \eta C_{L_\alpha} q S_t l \, 4 R \psi_F^2 \quad \text{per cycle}$$

The energy W_D dissipated per cycle by the normal damping is (Ref 11)

$$dW = b\dot{\psi} \, d\psi; \quad \dot{\psi} = \psi_0 \omega \cos \omega t; \quad d\psi = \psi_0 \cos \omega t \, d(\omega t); \quad b = C_{L_\alpha} q S_t \frac{l^2}{U}$$

$$W_D = \int_0^{2\pi} b \psi_0^2 \omega \cos^2 \omega t \, d(\omega t) = \pi \omega b \psi_0^2 = \pi \omega \psi_0^2 \eta C_{L_\alpha} q S_t \frac{l^2}{U} \quad \text{per cycle.}$$

Equating W_D and W_F and solving for ψ_F, determines the condition for which the oscillation is undamped.

$$\frac{\psi_F}{\psi_0} = \sqrt{\frac{\pi \omega l}{4RU}}$$

The maximum allowable friction hinge moment is equal to the aerodynamic hinge moment associated with $\psi_F = \beta_F / R$

$$FHM_{max} = C_{H\beta} R \psi_F q S_t c_r = \sqrt{\frac{\pi \omega l}{4RU}} \; \psi_0 C_{H\beta} R q S_t c_r$$

Example: 1500-lb airplane, $\omega = \pi$ rad/sec, $l = 15$ ft, U = 150 ft/sec, q = 27 lb/sq ft., $C_{H\beta} = 0.04$, R = 0.10, S_t = 15 sq. ft, c_r = 2 ft, $\psi_0 = 1^\circ$. Bearing Friction $\frac{1}{2}\%$.

Then $FHM_{(Max.allow)} = \sqrt{\frac{\pi^2 15}{4 \cdot 150 \cdot .10}} \; \frac{\psi_0}{57.3} \; \frac{0.04}{10} \; 27 \cdot 15 \cdot 2 = .089 \psi_0 \text{ ft.lb/}_0 = 1.07 \psi_0 \text{ in lb/}_0$

Assuming a value of bearing friction of $\frac{1}{2}\%$, the actual (estimated) FHM would be FHM (Est. actual = .005 x (10 lb) x (0.5 in) = .025 in lb, based on a combined drag and weight loading of 10 lbs. acting on the rudder bearings, and a bearing radius of 0.5 inches.

The above calculations indicate that the friction would cause an undamped oscillation of about $\psi_0 = .025/1.07 = .024$ degrees amplitude, which would be imperceptible to the occupants of the airplane. It is necessary to safeguard against excessive friction, but if this is done, good results may be expected from the coupled surface.

D. Manual Control System

The friction of the control system must be separated from that of the coupled surface. One method of control is attained through the coupling linkage, as shown schematically in Fig. 17. The coupled surface must be held rigidly at A by an irreversible mechanism, in the absence of which the angle of yaw ψ would cause the entire surface to tip until stopped by limits, without moving the rudder. The control motion actuated by rudder pedals or hand crank through an irreversible mechanism at A would pull the rudder over for directional trim. The manual rudder control may then be considered as only a directional trimming device, since the power of the coupled surface requires no pilot control of the rudder, but permits two-control operation of the airplane, in which turning is accomplished by properly designed aileron control.

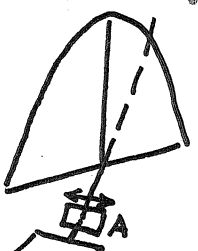

Fig 17 Manual Control of Coupled Fin & Rudder

If the horizontal tail is also coupled, longitudinal speed control may be accomplished in a manner similar to the directional control (cf.Fig.17) thus providing the ultimate simplicity for airplane control; a wheel for turning with appropriate angle of bank and means for airspeed adjustment and for directional trim.

VI. Summary and Conclusions

A. Application of Design Data

In order to design stabilizers using the principles of coupled surfaces, it is necessary to obtain values of the positions of the following items with respect to the rudder-hinge line and the tip-hinge line, in order to accurately place the node line on the surface:

1. Centers of gravity of fin and rudder.
2. Centers of pressure of fin and rudder due to α.
3. Centers of pressure of fin and rudder due to β.

These data may then be converted by simple calculations (cf. App. B and Figs. 18 and 19) into z, z_α, z_β etc., necessary for computing the tail efficiency and stability characteristics.

The variation to be expected in these data needs to be considered before final determination of the coupling ratio R may be accomplished. The effects of wear and service life should be determined, as well as Reynolds number and compressibility effects throughout the expected range of operation. Some of the variation factors may need to be determined by flight tests of a conservatively designed coupled tail with adjustable coupling ratio R.

Transonic airfoil data may be obtained by use of a wind tunnel with "bump." Such data will be very useful in the adaptation of coupled surfaces to supersonic vehicles (cf. Fig. 19). Supersonic data may be readily obtained at various Mach numbers (cf. Fig. 20) in the operating range. Preliminary calculations indicate that a considerable reduction in tail area may be effected in rocket vehicles designed for $M \doteq 3$ (cf. Fig. 21). by providing for the control to be fixed for M<1, and coupled thereafter.

When the necessary design information is available, the determination of coupling ratio R and tail efficiency η_s and η_D are easily accomplished (cf. App. B).

Fig. 18 Design of Coupled Tail for Transport Airplane

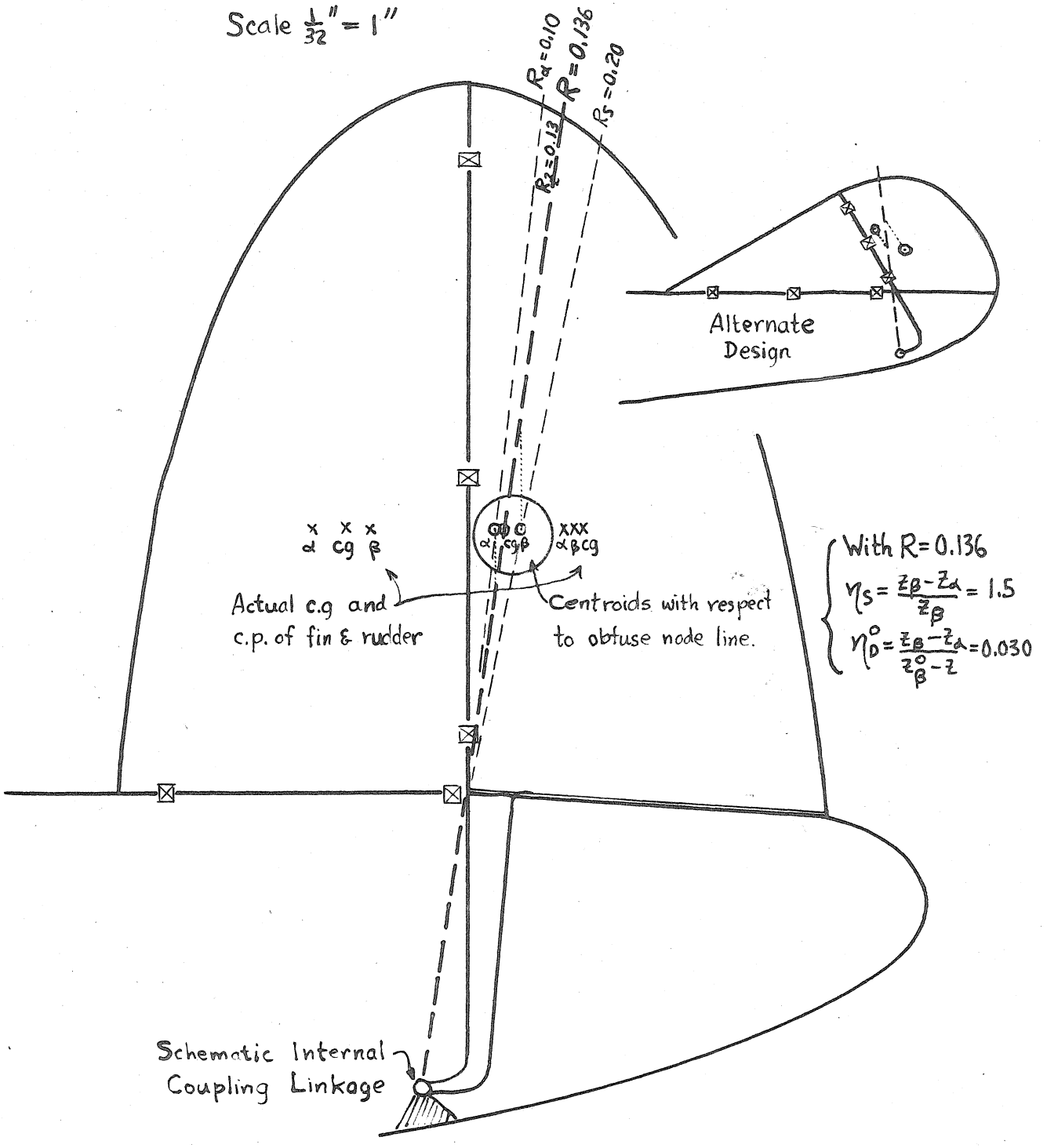

c.p. of / Due to	Fin				Rudder				$Q = V_1 z_1 / V_2 z_2$	$R_o = R_2 / 1+Q$
	x_1	z_1	R_1	V_1	x_2	z_2	R_2	V_2		
α	1.05	-1.75	-0.60	0.75	-0.70	-1.75	0.40	0.25	+3.00	0.10
β	0.70	-1.75	-0.40	0.50	-0.70	-1.75	0.40	0.50	+1.00	0.20
c.g.	0.83	-1.75	-0.48	0.70	-0.75	-1.75	0.43	0.30	+2.30	0.13

Subsonic: $\eta_s = 1.0$ (fixed @ M<1)

Supersonic; $\eta_s = 1 + \frac{.27}{.18} = 2.5$ @ $M = \infty$

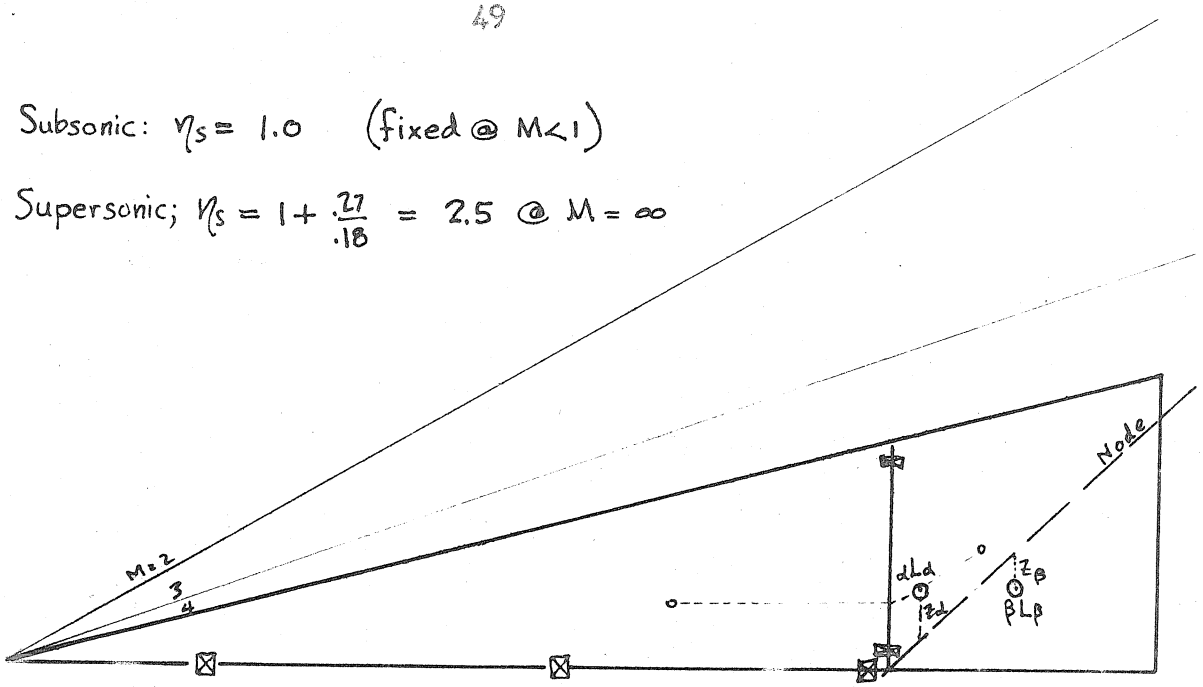

Fig. 19 Design of Coupled Tail for Supersonic Speeds
(To be stable at all speeds M>1)

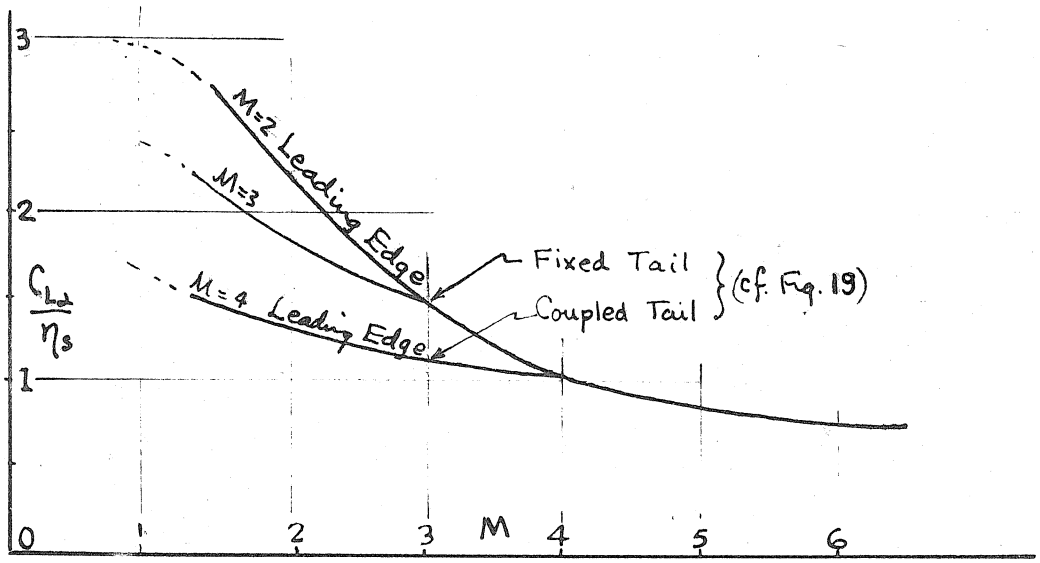

Fig. 20 Tail Effect vs. Mach Number

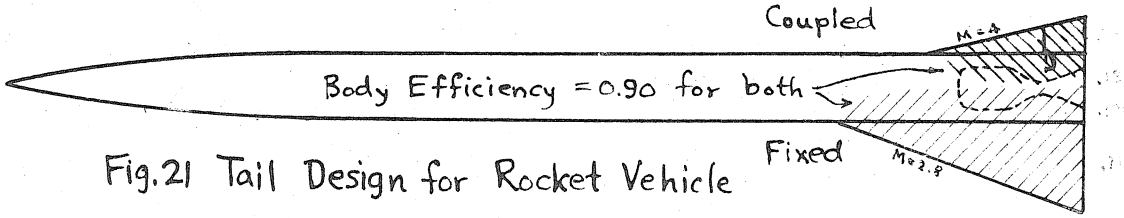

Fig. 21 Tail Design for Rocket Vehicle

Coupled Tail $\eta_s = 2.5$ @ $M = 3$
Ratio of Tail Areas $\frac{\text{Coupled}}{\text{Fixed}} \doteq 0.37$ for Equal Static Stability
$[C_{L\alpha}\, \eta_s (S_t + S_b)]$

For airplanes designed to fly at high altitudes, the time to damp to one-half amplitude of an airplane equipped with a coupled tail is less than that of a fixed control airplane, the ratio being 1: η_s (cf. Table II), and the ratio of critical damping 1: $\sqrt{\eta_s}$. An aerodynamic solution is thus made available for a hitherto troublesome problem, (cf. Ref. 12) which has been solved by automatic pilot means. The alternative aerodynamic solution may sometimes be more desirable.

In order to attain satisfactory results with the coupled tail, the surface configuration, airfoil contours, mass balance terms, coupling linkage, etc. must be in the correct proportions. Normal methods of construction are considered to be satisfactory in general, providing the design requirements for the coupled tail are met.

From the weight standpoint, a comparison may be made between the weight increase due to additional hinges and coupling linkage and the weight decrease due to smaller surface and lower span. Although no actual weight calculations have been made, it is believed that, for a given stabilizing effect, the coupled tail may be produced at a considerably lower weight than a normal tail.

By use of these methods, it is possible to design stabilizing surfaces that are many times more effective than fixed surfaces of equal area. A good design may be expected to give a tail efficiency $\eta_s = 6$ (cf. App B). However, a large value of η_s is not essential, since great improvement in the airplane stability may be effected by use of $\eta_s = 1.5$ as shown by the numerical example for the transport airplane (cf. Sec. V-B). The beneficial effect is derived from the control moments exerted on the airplane rather than high static stability.

When compared with a normal free rudder, with its downstream floating tendency, the coupled surface will restore equilibrium conditions

much more quickly after displacement. It will behave essentially like an automatic stabilizer. For this reason, properly designed coupled surfaces may be called automatic control surfaces.

B. Conclusions

Automatic or coupled control surfaces, designed and built by the methods described, should be practical, serviceable devices for use on many types of aircraft.

Coupled surfaces will provide greater riding comfort and proper free control stability for aircraft and rocket vehicles of the future.

From the standpoint of stability, it appears that the coupled tail having a static tail efficiency of only 1.5 results in the desired nearly aperiodic damping of long period disturbances.

The principle of coupled surfaces is applicable to supersonic vehicles as well as to subsonic, by maintaining the surfaces fixed during the subsonic flight, and free at supersonic speeds.

The economic effect of such a device on aircraft stability seems to justify the expenditure of considerable funds and effort in broadening the knowledge contained herein with regard to the design of vertical and horizontal tails, with consideration for the structural and weight aspects of the problem and refinements of configuration to result in higher efficiency.

References

1. Kendrick, J. B. "Coupled Surfaces," Journal of the Aeronautical Sciences, 13 (No. 6), June 1946

2. Lanchester, F. W., Aerodonetics, New York: Van Nostrand Company, 1910.

3. Gilruth, R. R., Requirements for Satisfactory Flying Qualities of Airplanes, Technical Report TR 775. Langley Field, (Va.): National Advisory Committee for Aeronautics, 1943.

4. Kendrick, J. B., Aero-Economics, 75-page booklet, a personal publication while at Graduate School of Aeronautics, California Institute of Technology, November 1945.

5. Jones, R. T., and Kleckner, H. F., Theory and Preliminary Flight Tests of an All-Movable Vertical Tail Surface, Advanced Restricted Report, Langley Field, (Va.): National Advisory Committee for Aeronautics, January 1943.

6. von Karman, T., and Biot, M.A., Mathematical Methods in Engineering. New York: McGraw Hill Book Company, 1940.

7. Kendrick, J. B., Automatic Control Surfaces, Aerodynamic Document No. AD-1029. Burbank, (Calif.): Lockheed Aircraft Corporation, March 1945.

8. Smith, E. S., Automatic Control Engineering. New York: McGraw Hill Book Company, 1940.

9. Den Hartog, J. P., Mechanical Vibrations. New York: McGraw Hill Book Company, 1940.

10. Koppen, O. C., Longitudinal and Lateral Stability. Cambridge: Massachusetts Institute of Technology Classroom Notes, 1934.

11. Draper, C. S., Aircraft Instruments. Cambridge: Massachusetts Institute of Technology Class Notes, 1936.

12. White, R. J., "Investigation of Lateral Dynamic Stability of XB-47 Airplane," Journal of Aeronautical Sciences, 17 (No. 3) March 1950.

Definition of Terms*

A, B, C, D, E } quartic coefficients (cf Eqs. 13)

c = average chord of tail

c_r = average rudder chord

C_H = Hinge moment coefficient; $C_{H_\alpha} = \frac{dC_H}{d\alpha}$; $C_{H_\beta} = \frac{dC_H}{d\beta}$

C_L = Lift$/qS$; $C_{L_\alpha} = \frac{dC_L}{d\alpha}$

c_{p_α} = center of pressure of α - produced forces

c_{p_β} = center of pressure of β - produced forces

c_g = center of gravity

I, J, K } defined in Eqs. 13

$h_\alpha = C_{H_\alpha} S_r c_r / C_{L_\alpha} S z_t$

$h_\beta = C_{H_\beta} S_r c_r / C_{L_\alpha} S z_t$

$\Sigma m_i z_i^2 = I_n$ = "moment of inertia" of tail about node line. (cf Fig. 12)

$\Sigma m_i x_i^2 = I_a$ = moment of inertia of tail and airplane about airplane c.g.

$k = L_{\beta_r} / L_\beta$ = fraction of lift on rudder

$k = I_a / m x^2$

$L_\alpha = C_{L_\alpha} qS$

$L = C_{L_\alpha} / k$

m = total mass of tail

$q = \rho U^2/2$ = dynamic pressure

$\Sigma m_i x_i z_i = P$ = "product of inertia" of tail about node line and c_g(airplane)

R = coupling ratio = $\gamma/\beta = x_l/z_l$

R_α, R_z, $R_S = R_\beta$ } defined in App. B

$\mathcal{R}$ = Routh's discriminant (cf Eq. 15)

S = tail area

S_r = rudder area

U = air velocity

x = c.g. (airplane) to rudder hinge line

* Stability derivatives are defined in Tables III and V.

Definition of Terms
(continued)

x_1, x_2, x_3, x_4
z_1, z_2, z_3, z_4 } See p. 13

x_α = rudder hinge to α - centroid
x_β = rudder hinge to β - centroid
$x_4 = x_{\beta r}$ = rudder hinge to rudder c.p.
x_ℓ = rudder hinge to linkage attachment point
z = node line to centroid of mass of tail.

z_α = node line to α - centroid } (cf Eqs. 18)
z_β = node line to β - centroid }
z_ℓ = tip hinge to linkage attachment point
α = angle of attack
β = rudder deflection angle
γ = tip deflection angle
η_s = static tail efficiency
η_D = dynamic tail efficiency

$\lambda = d/dt$

ρ = Air mass density
$\tau = \frac{d(\text{lift per unit of } \beta)}{d(\text{lift per unit of } \alpha)}$
ψ = angle of yaw
ζ = ratio of damping to critical damping $= (b/2a)\left(\sqrt{\frac{a}{c}}\right)$

Appendix A

Aero-Economic Considerations

In order to consider the economic advantages of stability, one might specify certain minimum requirements to be met, which may be condensed into the following: hands-off operation and satisfactory trim over a reasonable speed range; disturbances nonviolent, or damped in reasonable length of time; and satisfactory behavior in stall with and without power, flaps, etc. After a standard set of requirements has been established, the economic consequence of departures from this standard may then be considered, as a means to determine the relative importance of various design parameters. Certain procedures have been developed (cf. Ref. 4) for the evaluation of many factors concerned with transport airplane operation, which will be of value in the study. Although it is difficult to apply the aero-economic philosophy to private or military airplanes, which do not often consider such factors as the seat-mile cost, still the economic principles hold true as well as for an air carrier, since some one must eventually pay all the costs of operation; hence, the air transport may be used as a rough indication of the economic aspects of the family airplane and the military airplane.

The "value of a pound" is a common factor in air transport operation. A pound less weight empty makes available a pound more payload, with its integrated revenue over the life of the airplane. The value of a pound varies widely with the type of airplane, nature of operations, etc., but an average value is about $200 per pound.

Experiences has shown that, if the vertical tail area is sufficient to provide only slight directional stability, then the stalling characteristics of the airplane will be poor and minimum speed landings at V_L will not be practical. Landings will be made at somewhat higher speed,

$V_L + \Delta V$, at which condition the airplane will feel safe to the average pilot. The amount of wing area, or $C_{L_{max}}$, which is wasted by inability to make minimum speed landings is evaluated by reference to Fig. 22. It may be desirable to increase the vertical tail area or efficiency, perhaps at the expense of the wing area, in order to effect the best compromise and the lowest normal landing speed. Increased vertical tail area will permit slower, steeper glides and shorter takeoff and landing distances over an obstacle (cf. Fig. 23). Savings in ground time by reducing the takeoff and landing distance should also be considered an important advantage of the airplane which is able to approach and land at slower speed (cf. Fig. 24).

With the foregoing means available to calculate aero-economic values, the following transport airplanes (cf. Table VI) may be compared. Consider an airplane B with a coupled tail twice as powerful as that of the standard airplane A which barely meets the stability specification. A weight saving of 50 pounds might be effected by reducing the tail area of airplane B, amounting to 50 x 200 = $10,000 per airplane increase in aero-economic potential. However, this value is small compared with the potential to be gained by shorter takeoff and landing distance and by reduced landing speed (if there is a premium on it); hence it may be concluded that maximum economic value is gained by utilizing a high degree of stability in the transport design. The possibility of using smaller airports in the operation of airplane B than are practical for the performance of airplane A may prove to be of great economic importance. It is not unlikely that a 10 per cent improvement in takeoff and landing distance may be effected by a 100 per cent increase in tail effectiveness. The increased earning power of the airplane due to this improvement alone might easily exceed the initial cost of the airplane.

It is therefore evident that the provision of high stability is of great economic as well as technical importance in aircraft design and operation.

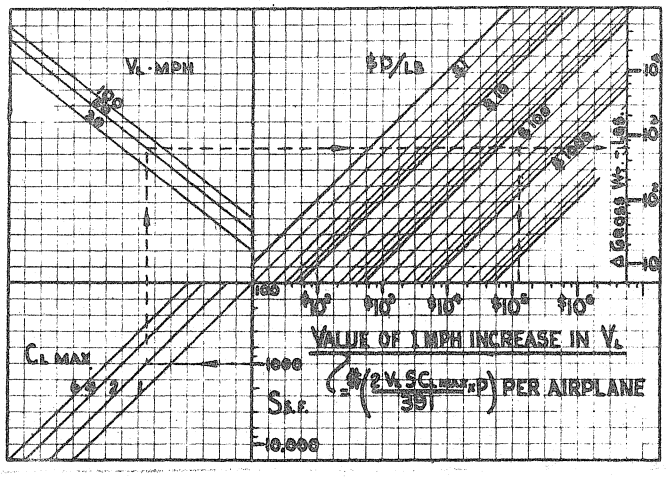

Fig. 22 One MPH Increase in Permissible Landing Speed

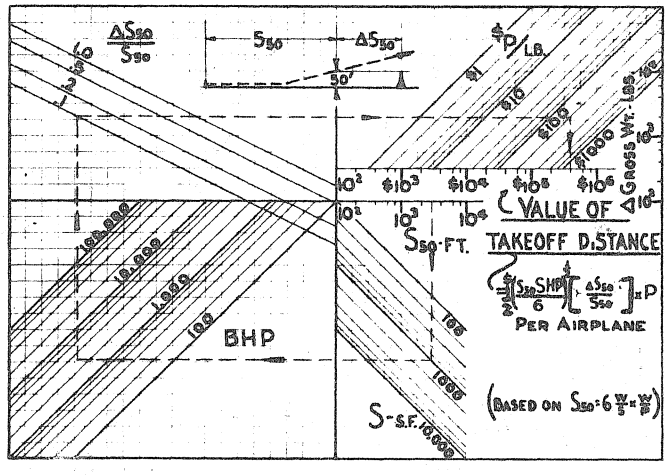

Fig. 23 Takeoff Distance and Obstacle Clearance

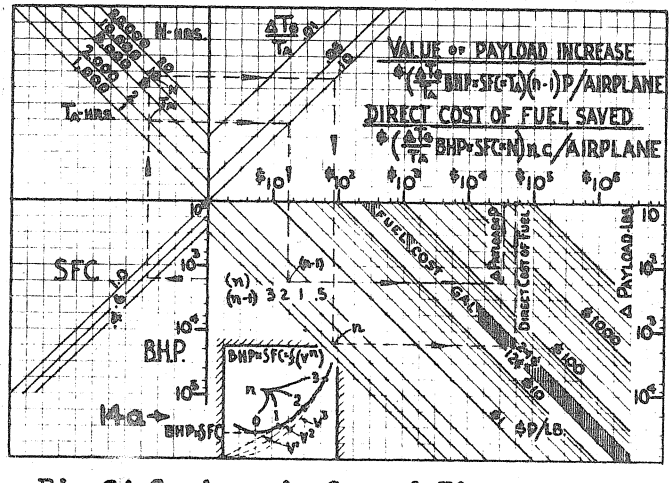

Fig. 24 Savings in Ground Time

Table VI

Aero-Economic Values for Aircraft Stability

Airplane Data		Operation Data	
Wing area	1000 sq ft	Rate per ton-mile	$ 0.20
$C_{L_{MAX}}$	2.0	Gross revenue/airplane	$ 1.5 x 10^6
Landing speed	60 mph	Normal life	10,000 hrs
Brake hp	3000	Average air time	2 hrs

Aero-Economic Data (cf. Ref. 4)

Value of a pound	$ 200/lb/airplane*
Value of 1 mph lower landing speed	$100,000/airplane*
Value of 1 per cent shorter takeoff distance over obstacle	$ 40,000/airplane*
Value of 1 per cent reduction in ground handling time/air time	$ 10,000/airplane*

* The actual values obtained from such analysis are subject to wide variations because of airline regulations, type of service, and many other factors. The values shown are intended as a rough approximation only of the aero-economic trend.

Appendix B

Data Required for Design

The centroids of the coupled surface may be determined from wind tunnel tests in the following manner:

$$(x_\alpha, z_{t_\alpha}) = \left(\frac{d(\text{pitching moment})/d\alpha}{d(\text{side force})/d\alpha}, \frac{d(\text{tipping moment})/d\alpha}{d(\text{side force})/d\alpha}\right)$$

$$(x_\beta, z_{t_\beta}) = \left(\frac{d(\text{pitching moment})/d\beta}{d(\text{side force})/d\beta}, \frac{d(\text{tipping moment})/d\beta}{d(\text{side force})/d\beta}\right)$$

The chordwise distributions may be assumed from normal airfoil theory and checked by rudder hinge-moment measurements. Fin and rudder distribution may be directly determined by a strain-gage arrangement which measures rudder side force and hinge moment. The latter method is preferable because of greater accuracy. Mass effects may be found by calculation or by weighing the parts.

Measurement of centroid positions from the obtuse node line, which simplified the dynamic stability development, involves a singularity as $R \to 0$, at which condition the centroids of the rudder approach ∞ * and items like z, z_α and z_β vary with R, the node position as shown in Fig. 25, where

$$z = cg\left(1 - \frac{R_z}{R}\right)$$

$$z_\alpha = z_{t_\alpha}\left(1 - \frac{R_\alpha}{R}\right)$$

$$z_\beta = z_{t_\beta}\left(1 - \frac{R_s}{R}\right)$$

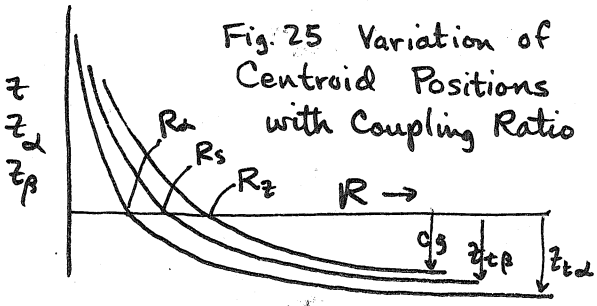

Fig. 25 Variation of Centroid Positions with Coupling Ratio

cg., z_{t_α} and z_{t_β} are the center of gravity, center of pressure of α- produced forces, and center of pressure of β-produced forces respectively, with respect to the tip-hinge line at the base of the fin, to be determined by test or calculation. The values of R where z, z_α and z_β become zero may be found when the individual values of c.p. or c.g. of fin and rudder are determined, and their relative strengths are denoted by V_1 and V_2 respectively. In other words, the values of R_o represent lines radiating from the origin through the centroids of the fin and rudder forces (due to α, β or inertia) with respect to the bent node line. The method of determining R_o is as follows:

Given $V_1 @ (x_1 = 0, z_1)$ and $V_2 @ (x_2, z_2)$ $\Rightarrow$ $V_1 + V_2 @ \left(\frac{V_2}{V_1+V_2} x_2, \frac{V_1 z_1 + V_2 z_2}{V_1 + V_2}\right)$ Coords from rhl and thl.

Coordinates from rhl and node: $V_1 + V_2 @ \left(\frac{V_2}{V_1+V_2} x_2, \frac{V_1 z_1 + V_2 z_2 - V_2 \frac{x_2}{R}}{V_1 + V_2}\right)$

* If the rudder hinge line is not perpendicular to the tip hinge, z, z_α and z_β will approach definite values as $R \to$ rudder hinge line.

Condition for node through centroid of V_1+V_2 : $V_1 z_1 + V_2 z_2 - V_2 \frac{x_2}{R} = 0$

$$\therefore R_0 = \frac{R_2}{1+\frac{V_1 z_1}{V_2 z_2}} = \frac{R_2}{1+Q} \; ; \quad Q = \frac{V_1 z_1}{V_2 z_2} \; , \quad R_2 = \frac{x_2}{z_2}$$

The calculation of R_α, R_s and R_t may now be performed.

$$R_\alpha = \frac{x_3/z_3}{1+\frac{L_1 z_1}{L_3 z_3}} \; ; \quad R_s = \frac{x_4/z_4}{1+\frac{L_2 z_2}{L_4 z_4}} \; ; \quad R_t = \frac{x_r/z_r}{1+\frac{W_f z_f}{W_r z_r}}$$

One concludes that after certain basic information on mass distribution and aerodynamic properties is available, the dynamic stability criteria may be readily applied. The required conditions may be easily met by normal production methods and tolerances, permitting the attainment of coupled surfaces of high efficiency as illustrated by the examples given in the table below. However, it is not essential to the success of the coupled tail that extremely high values of η_s be obtained. The beneficial effect is derived from the phase of the control moments exerted on the airplane, rather than high static stability. This fact is proved in Section V-B where a value of $\eta_s = 1.5$ is shown to greatly improve the stability of a transport airplane.

Table VII. Estimate of Tail Efficiency

		Normal Practice	Slight Extra Care
Tolerance on	x_β	$-0.03c$	$-0.015c$
Therefore	z_β	$+0.20c$	$+0.10c$
	ε	$-0.10c$	$-0.05c$
	z_α	$-0.50c$	$-0.50c$
	η_s	$\frac{0.50+0.20}{0.20} = 3.5$	$\frac{0.50+0.10}{0.10} = 6.0$
$\frac{I_\alpha}{mx^2} = 1$,	η_0	$\frac{0.50+0.20}{0.10+0.20} = 2.33$	$\frac{0.50+0.10}{0.15} = 4.0$
$\frac{I_\alpha}{mx^2} = 50$,	η_0	$\frac{0.30+0.20}{0.10+0.20\times 50} = 0.069$	$\frac{0.50+0.10}{0.10+0.10\times 50} = 0.12$

Appendix C

Different Ways of Deriving Static Equilibrium

Three methods will now be used for determining the static equilibrium of the coupled surfaces, all leading to the same answer but illustrating different aspects of the mechanics.

(1) Equilibrium of Moments about r.h.l. and t.h.l. Since the forces acting on the fin do not contribute to the rudder hinge moment because of the restraint exerted by the tip hinge, the rudder hinge moment may be taken with or without the fin forces. In other words, since $x_1 = x_2 = 0$, $L_\alpha x_\alpha = L_1 x_1 + L_3 x_3 = L_3 x_3$ and $L_\beta x_\beta = L_2 x_2 + L_4 x_4 = L_4 x_4$.

	Including Case I Fin Forces	Excluding Case II Fin Forces	Excluding Case III Fin Forces
$\sum M_{rhl}^{(1)} = 0$	$\psi L_\alpha x_\alpha + \beta L_\beta x_\beta = F x_\ell$	$\psi L_3 x_3 + \beta L_4 x_4 = F x_\ell$	$(C_{h_\alpha}\psi + C_{h_\beta}\beta)\, q S_r c_r = F x_\ell$
$\sum M_{thl}^{(2)} = 0$	$\psi L_\alpha z_{t_\alpha} + \beta L_\beta z_{t_\beta} = F z_\ell$	$\psi(L_1 z_1 + L_3 z_3) + \beta(L_2 z_2 + L_4 z_4) = F z_\ell$	$C_{L_\alpha} z_t q S(\psi + \tau\beta) = F z_\ell$ (Assuming $z_t = z_1 = z_2 = z_3 = z_4$)
(1)/(2) *	$\dfrac{\psi x_\alpha + \tau\beta x_\beta}{\psi z_{t_\alpha} + \tau\beta z_{t_\beta}} = R$	$\dfrac{\psi L_3 x_3 + \beta L_4 x_4}{\psi L_\alpha z_{t_\alpha} + \beta\tau L_\alpha z_{t_\beta}} = R$	$\dfrac{C_{h_\alpha}\psi + C_{h_\beta}\beta\left(\frac{S_r c_r}{C_{L_\alpha} S z_t}\right)}{\psi + \tau\beta} = R$
β/ψ	$(+)\frac{1}{\tau}\left(\frac{R z_{t_\alpha} - x_\alpha}{R z_{t_\beta} - x_\beta}\right) = -\frac{1}{\tau}\frac{z_\alpha}{z_\beta}$ cf Fig 26	$-\frac{1}{\tau}\left(\frac{R z_{t_\alpha} - L_3 x_3/L_\alpha}{R z_{t_\beta} - L_4 x_4/L_\beta}\right) \doteq$	$-\frac{1}{\tau}\left(\frac{R - h_\alpha}{R - h_\beta/\tau}\right)$ (cf Ref 1)
Singular Point	$R_s = \frac{x_\beta}{z_\beta}$; ie $z_\beta = 0$	$R_s = \frac{L_4 x_4}{L_\beta z_{t_\beta}} = \frac{x_\beta}{z_{t_\beta}} \doteq$	$R_s = \frac{h_\beta}{\tau} = \frac{L_4 z_4}{L_\beta z_t} = \frac{x_\beta}{z_t}$

* $L_\beta = \tau L_\alpha$, $L_1 z_1 + L_3 z_3 = L_\alpha z_{t_\alpha}$, $L_2 z_2 + L_4 z_4 = \tau L_\alpha z_{t_\beta}$

In each case, $R = \dfrac{\psi M_{r_\alpha} + \beta M_{r_\beta}}{\psi M_{t_\alpha} + \beta M_{t_\beta}}$. Then $\dfrac{\beta}{\psi} = -\dfrac{R M_{t_\alpha} - M_{r_\alpha}}{R M_{t_\beta} - M_{r_\beta}}$ and $R_s = \dfrac{M_{r_\beta}}{M_{t_\beta}}$

In Case I, the form of the ratio β/ψ is simplified by reference to the similar triangles in Fig. 26a. This form is found to be most convenient for later work.

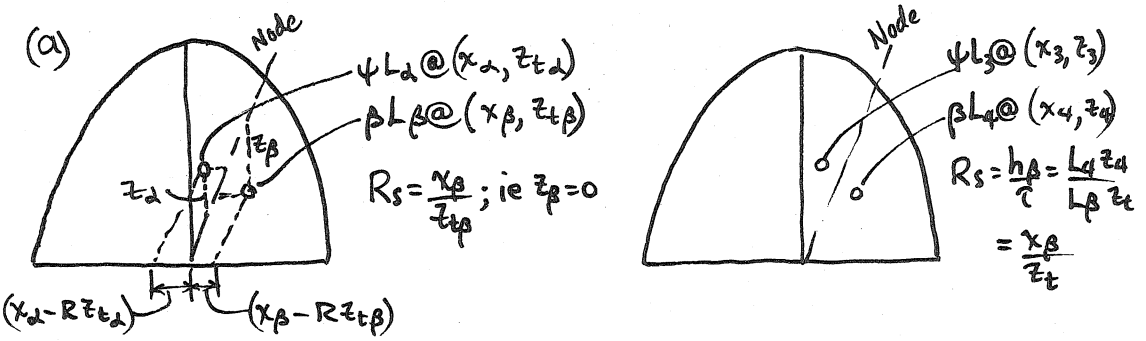

Fig. 26. Centroids of Rudder Produced Forces Determine Critical Coupling Ratio R_s

In Case I, the critical coupling ratio R_s passes through the centroid of βL_β

In Cases II and III, R_s must lie well forward of the c.p. of βL_4, since $|x_\beta| < |x_4|$

(2) Equilibrium of Moments about Node Line. For static equilibrium, $F = \psi L_\alpha + \beta L_\beta$ and $\Sigma M_{node} = 0$. The moment of F is zero with respect to the node line; hence

$$\Sigma M_{node} = 0\,; \quad \psi L_\alpha z_\alpha + \beta L_\beta z_\beta = L_\alpha (\psi z_\alpha + \tau \beta z_\beta) = 0$$

The value of L_α is arbitrary and not necessarily zero, so

$$\psi z_\alpha + \tau \beta z_\beta = 0\,, \quad \frac{\beta}{\psi} = -\frac{1}{\tau}\frac{z_\alpha}{z_\beta} \quad \text{as in Case I}$$

(3) Energy Method. Lateral deflections with respect to the plane of symmetry are $-z_i \gamma$, z_i being measured from the node line (cf. Fig. 7 and Eq. 4). The static equilibrium position is found by minimizing the potential energy E as follows:

$$E = (L_\alpha z_\alpha \psi + L_\beta z_\beta \beta)\gamma$$

$$\frac{dE}{d\gamma} = L_\alpha (z_\alpha \psi + \tau z_\beta \beta) = 0\,; \quad \therefore \frac{\beta}{\psi} = -\frac{1}{\tau}\frac{z_\alpha}{z_\beta} \text{ as before.}$$

Appendix D

Correlation of Wind Tunnel Model Tests with Theory

Tests of Small Fin and Rudder

Following the concept and original analysis of the static stability of coupled surfaces (cf. Fig. 27), a solid mahogany vertical tail and end plate were made for wind-tunnel tests (cf. Fig. 13). This model had a span of 11 inches and an area of 84 sq. in and was tested in a 2 x 3 ft. throat wind tunnel at a dynamic pressure of 40 lb/sq ft and a Reynolds number of about 10^6 based on the average chord.

Excellent agreement was obtained between the static stability theory and test results (cf. Fig. 28). The experimental points were obtained from free-control wind-tunnel tests of the coupled tail at various angles of yaw, as shown by the solid curves of Fig. 29. Rudder deflection tests performed in the usual manner (as shown dotted in Fig. 29), when cross-plotted for various linkage ratios, gave the same results as the coupled tail.

The small model was later mounted on the end of a 3-foot swinging arm in the 2 x 3 ft tunnel and subjected to dynamic stability tests (cf. Table VIII). These tests will be reported and analyzed later with tests of the larger model.

Table VIII

Dynamic Stability Tests on Small Model CFR-8

Test No.	R =	x_l/z_l	c. g.	Balance Configuration	Observed Stability*
3S	0.072	0.687/9.5	3.75	S	S_1
		0.326/4.5	"	S	S_3
7S	0.072	0.687/9.5	"	S+ rudder balance	S_2
2S	0.095	0.907/9.5	6.06	S + $4\frac{1}{2}$ in pennant	S_1
	0.095	0.907/9.5	3.75	S + rudder balance	U
4S	0.095	0.813/8.5	"	S	U ± 8°
	0.095	0.713/7.5	"	S	S_2
	0.095	0.622/6.5	"	S	N
1S	0.115	1.09/9.5	7.75	S + 12 in pennant	S_1
		0.46/4	6.06	+ $4\frac{1}{2}$ in pennant	S_3
5S	0.115	1.09/9.5	3.75	S	U
		0.92/8	"	S	U ± 14°
		0.69/6	"	S	U ± 8.5
		0.60/5.22	"	S	S_1
		0.46/4	"	S	S_2
	0.133	-0.281/-2.11	"	S	U
6S	0.161	0.56/3.5	"	S	U ± 15
		0.47/2.92	"	S	U ± 13
		0.37/2.32	"	S	U ± 5
		0.28/1.74	"	S	S_1
		"	6.06	S + $4\frac{1}{2}$ in pennant	S_3
		"	7.75	S + 12 in pennant	S_3
	0.182	0.73/4.0	3.75	S	U ± 16
	0.222	0.89/4.0	"	S	U ± 18

*Degrees amplitude of oscillation are shown as $U^{\pm}(\ )^{\circ}$

Increasing amounts of stability: U, N, S_1, S_2, S_3

Fig 27 Copy of Original Static Stability Theory

June 21, 1944

THEORY OF COUPLED FIN AND RUDDER

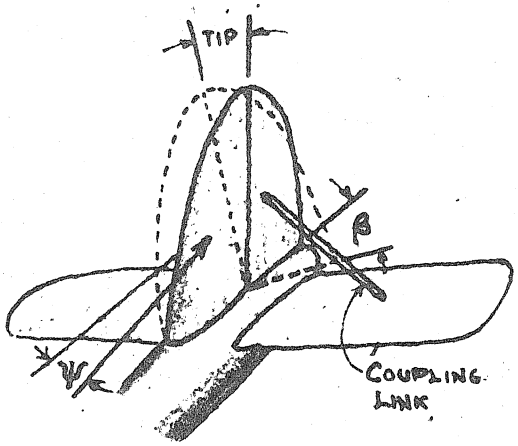

PRINCIPLE:

ANGLE OF YAW ψ CAUSES VERTICAL FIN TO TIP. COUPLING LINK BETWEEN RUDDER AND HORIZONTAL STABILIZER (OR OTHER SUITABLE POINT) CAUSES RUDDER TO DEFLECT β.

THE RESISTANCE TO SIDESLIP IS THEN MEASURED BY $\frac{dC_L}{d\psi} = \frac{dC_L}{d\alpha}(1+\tau\frac{\beta}{\psi})$

RESULT:

THE COUPLED FIN AND RUDDER IS THEREFORE $(1+\tau\frac{\beta}{\psi})$ TIMES AS EFFECTIVE AS A FIXED VERTICAL SURFACE OF EQUAL AREA.

THEORY:

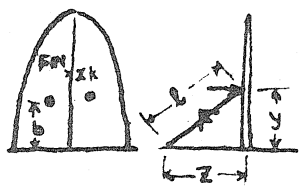

AERODYNAMIC TIPPING MOMENT = LINK RESTRAINING MOMENT

$$\frac{dC_L}{d\alpha}(\psi+\tau\beta)\, q\, S\, b = -F\,\frac{x}{l}\,y \qquad (1)$$

RUDDER HINGE MOMENT = LINK RESTRAINING MOMENT

$$\left(\frac{dC_h}{d\alpha}\psi + \frac{dC_h}{d\beta}\beta\right) q\, S_R C_R = -F\,\frac{z}{l}\,x \qquad (2)$$

DIVIDING (1) BY (2), AND SOLVING FOR $\frac{\beta}{\psi}$ —

$$\frac{y}{x} = \frac{(\psi+\tau\beta)\frac{dC_L}{d\alpha}\, S\, b}{\left(\frac{dC_h}{d\alpha}\psi + \frac{dC_h}{d\beta}\beta\right) S_R C_R}$$

$$\frac{\beta}{\psi} = (-)\frac{1 - \frac{y}{x}\frac{S_R}{S}\frac{C_R}{b}\frac{dC_h}{d\alpha}\Big/\frac{dC_L}{d\alpha}}{\tau - \frac{y}{x}\frac{S_R}{S}\frac{C_R}{b}\frac{dC_h}{d\beta}\Big/\frac{dC_L}{d\alpha}}$$, ~~SHOWN PLOTTED ON p.3~~

WHERE $\tau = \frac{d\sigma}{d\beta}$, $q = \frac{\rho}{2}V^2$, S = VERT. TAIL AREA

b = DISTANCE TO CENTROID OF TIPPING FORCES.

F = FORCE APPLIED BY LINK.

x, y, z = AS SHOWN, TO CENTROID OF RUDDER FORCES.

S_R = RUDDER AREA C_R = RUDDER MEAN CHORD.

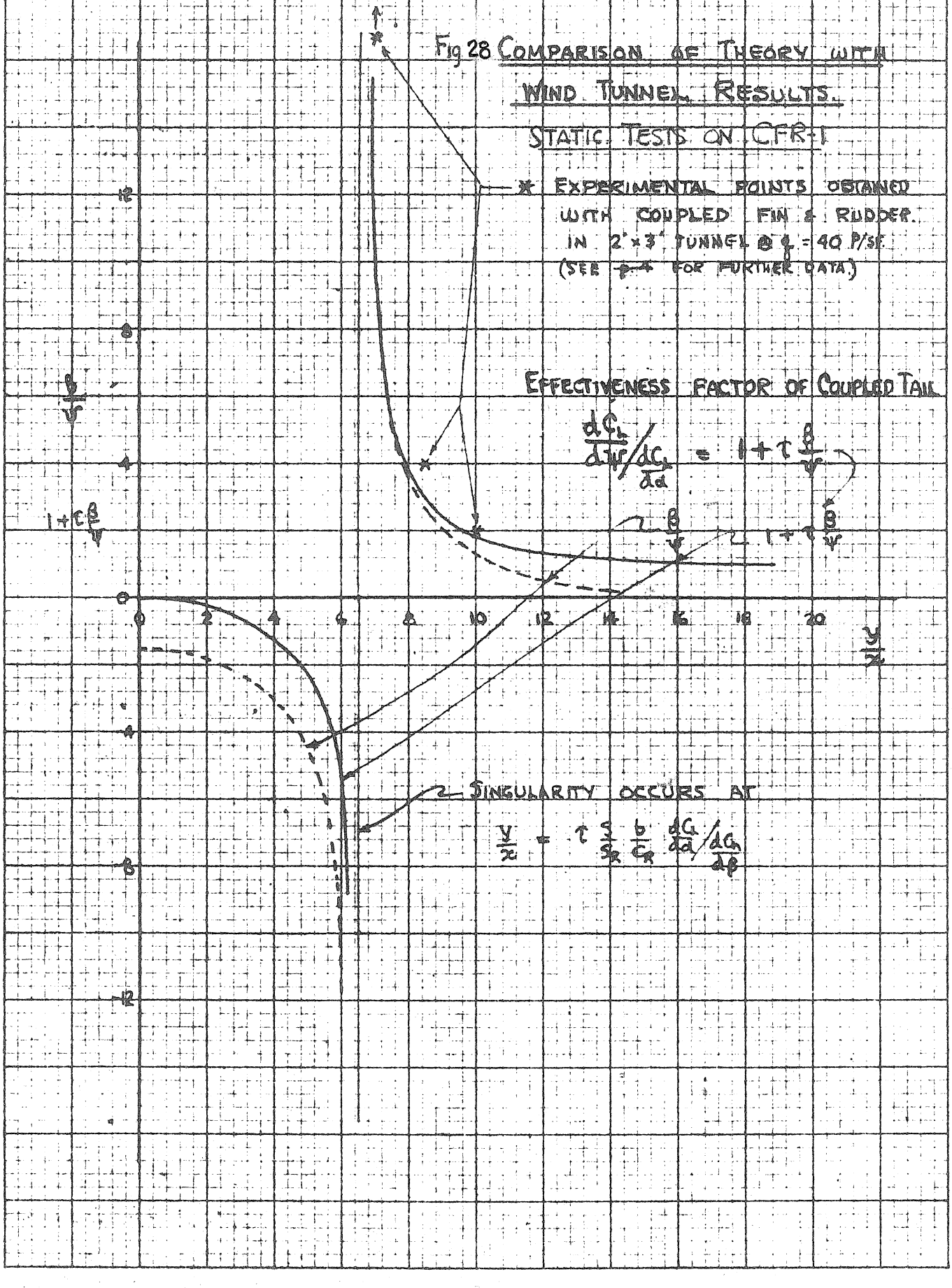
Fig 28 COMPARISON OF THEORY WITH WIND TUNNEL RESULTS.
STATIC TESTS ON CFR-1
* EXPERIMENTAL POINTS OBTAINED WITH COUPLED FIN & RUDDER. IN 2'×3' TUNNEL @ q = 40 P/SF.
(SEE p-4 FOR FURTHER DATA.)
EFFECTIVENESS FACTOR OF COUPLED TAIL
$\frac{d C_L}{d\psi} / \frac{dC_L}{d\alpha} = 1 + \tau \frac{\beta}{\psi}$
$\frac{\beta}{\psi}$
$1 + \tau \frac{\beta}{\psi}$
$1 + \tau \frac{\beta}{\psi}$
12
8
4
0
-4
-8
-12
0
2
4
6
8
10
12
14
16
18
20
$\frac{y}{x}$
SINGULARITY OCCURS AT
$\frac{V}{x} = \tau \frac{S}{S_R} \frac{b}{C_R} \frac{dC_L}{d\alpha} / \frac{dC_L}{d\beta}$

Fig 29 RESULTS OF WIND TUNNEL TEST

COUPLED FIN AND RUDDER

TESTS ON CFR-1

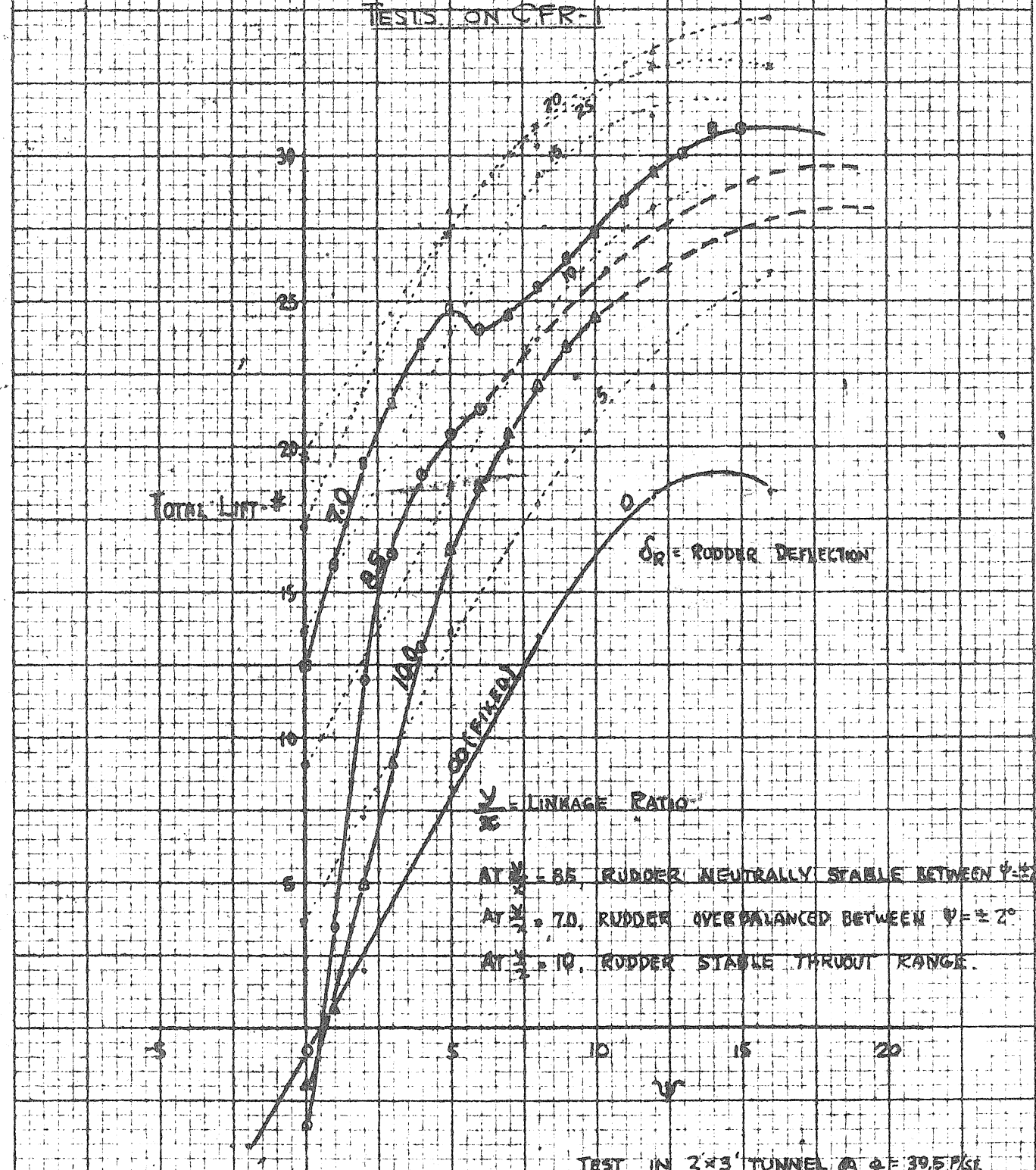

C. Tests of Large Fin and Rudder

After the encouraging results obtained with the small heavy model CFR-1, it was decided to build a larger model, approximately twice the scale of the first, of sheet-aluminum skin construction with wooden spars and ribs. This model had a span of 22 inches and an area of 2.64 sq ft. It was tested in a 5-foot-diameter wind tunnel at a dynamic pressure of about 9 lbs/sq ft, giving a Reynolds number of about 9×10^5. Static tests were made on CFR-2 (cf. Table II) and modifications thereof, as a means of perfecting of hinge-moment characteristics and increasing the static effectiveness of the coupled tail. The final configuration gave static tail efficiency more than eight times that of the fixed vertical tail (cf. Fig. 30). The experimental results with CFR-2 et al are described by notes taken during the test period, as follows:

CFR-2. Model CFR-2 of the coupled fin and rudder similar to the original design was mounted in the 5-foot tunnel on the regular balance trunnions. The experimental arrangement was unstable, and at angles of yaw the entire balance system and tail fluttered rather severely. The oscillation appeared* to be caused by resonance in the balance system and by irregular flow in the 5-foot tunnel. An attempt to repeat the results found previously on CFR-1 in the 2 x 3 ft tunnel by mounting CFR-1 on the same balance system in the 5-foot tunnel showed CFR-1 also to be unstable in the 5-foot tunnel.

CFR-2 was modified by cutting the model until the rudder had flat sides. It was hoped that this change in contour might stop the flutter by change of the hinge moments for relatively small rudder angles. The

* The difficulty was probably due to improper mass distribution, the importance of which was not fully recognized at the time these tests were conducted.

FIGURE 30

YAW CHARACTERISTICS - REVISED ½ SCALE CFR-2

LINKED VERTICAL TAIL

(R-P3 - FK)

CFR-2

Pat
9-16-44

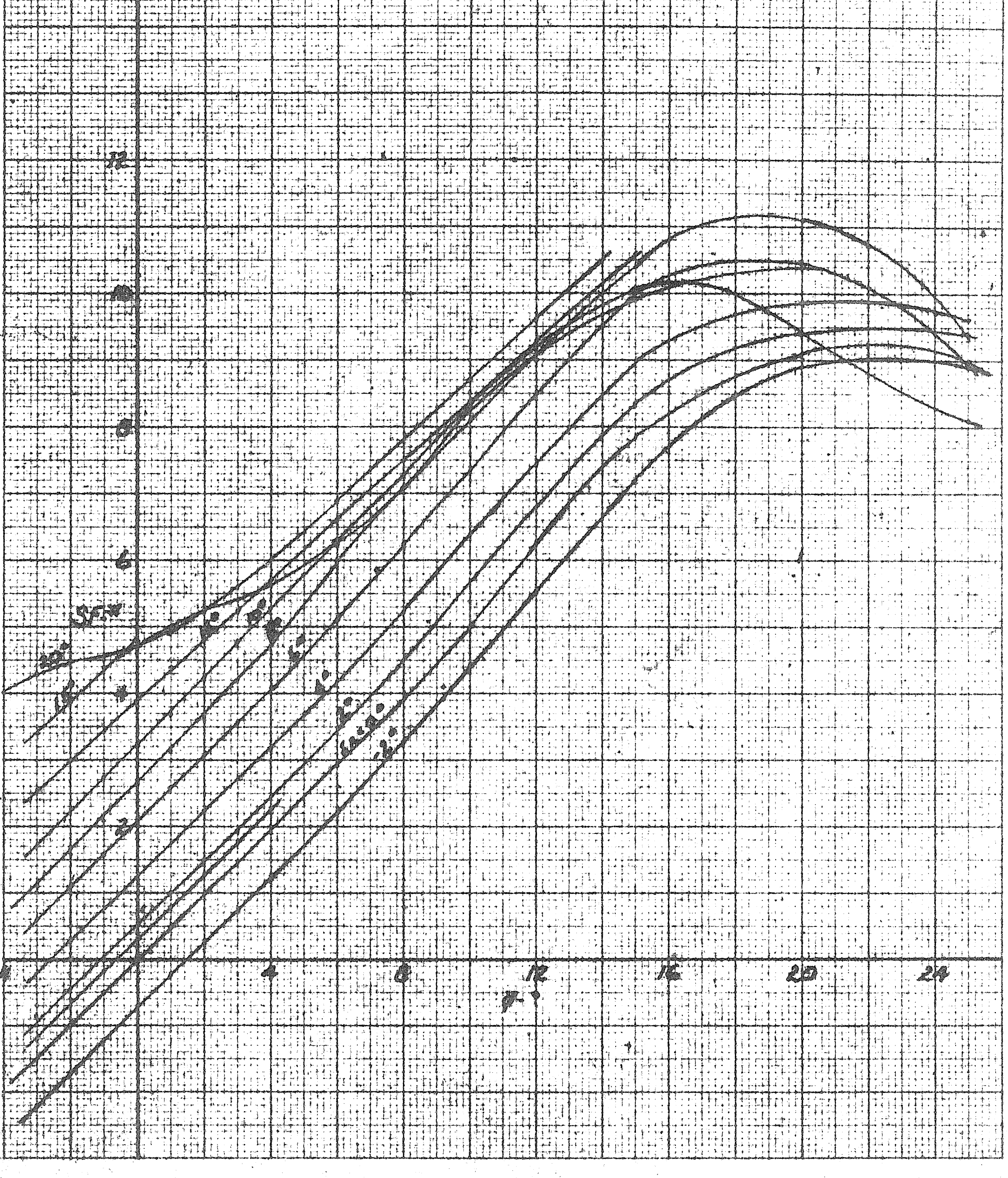

test showed no noticeable difference.

In attempting to correct this condition (tufts showed the tunnel flow to be quite irregular, and the entire rudder to be stalled for rudder and yaw angles of only 1 or 2 degrees), a honeycomb was installed in the 5-foot tunnel at the upstream end of the test section. Tufts placed in the empty tunnel showed that the honeycomb corrected the major part of the irregular flow.

With the honeycomb installed and the model CFR-2 mounted on the trunnions, the fixed rudder data shown on Fig. 30 were taken. When the rudder was fixed there was no flutter with this arrangement. It should be noted that these data (which are uncorrected for tunnel-wall effects) are considerably more consistent than any similar data taken previously in the same tunnel and on the same balance system.

The data plotted on Fig. 30 give the rudder effectiveness (side force slope with yaw) for several fixed rudder settings. It is to be noted that, for rudder deflections of 15°, the side force is less than that obtained for 8, 10, or 12° rudder, for angles of yaw greater than 4°. This condition is probably caused by separation on the large rudder and may be increased by the proximity of the tunnel walls.

Because of the method of operation of the coupled fin and rudder, this separation and consequent decrease in side force for larger rudder angles may be the reason for the oscillations. The rudder alone oscillated when the model was fixed to the tunnel floor with the fin and rudder coupled, but there was no flutter. The coupled rudder was aerodynamically overbalanced in this configuration.

Spoilers in the form of 3/32', 1/16', and 1/32-inch-diameter wire were fastened along the trailing edge of the rudder. By moving the rud-

der c.p. farther back, these spoilers removed all tendency of the coupled fin and rudder to flutter and to overbalance.

Referring to the coupled-tail theory (cf. Fig. 27), it is noted that the singular point where overbalance occurs is universally proportional to the hinge-moment curve slope. With the unfaired intersection of the flat rudder and fin and the rounded trailing edge of the rudder, the variations in hinge-moment curve slope with angle of rudder deflection were quite large. Thus, with the coupling ratio adjusted to give a large effectiveness factor at one rudder deflection, the rudder would be very much less effective at a greater rudder deflection.

From these observations, which are verified by the tests on CFR-4, 5, 6, and 7, one important fact of design is noted: A coupled fin and rudder to be designed for high effectiveness ratio must be aerodynamically designed to have linear hinge-moment vs rudder-deflection curve. Nonlinear curves might be usable if the variation from linearity is such as to cancel some variations in other factors, but the latter conditions would be extremely difficult to obtain. Therefore, in any design of a coupled fin and rudder, the aerodynamic features which produce linear hinge-moment curves should be used, i.e., constant centers of pressure.

CFR-4. Proceeding in this direction, the rounded trailing edge of CFR-3 was squared off by filling in with plasticine to make a blunt square trailing edge. This modification worked very well, being stable and not overbalanced.

CFR-5. CFR-4 was modified by faring in the fin and rudder. The rudder chord, a large percentage of the total (52%), had been flattened off, leaving a discontinuity in the airfoil slope at the intersection between fin and rudder. This intersection was modified to give a smooth

faired curve. (The trailing edge was squared by plasticine as for CFR-4.) The curves shown on Fig. 31 show very good results. Effectiveness ratios up to 7.8 can be obtained with the side-force curve slope nearly linear over a considerable range of angles of yaw. With the possible exception that the linear portion of the curves could be extended slightly, these curves are aerodynamically satisfactory.

CFR-6. Though (CFR-5 worked very well aerodynamically, it would require a squared-off trailing edge. From the structural and manufacturing standpoint the rounded trailing edge is desirable. CFR-6 was obtained by removing the plasticine from the trailing edge of CFR-5, giving a flat-sided rudder faired into the fin. The results obtained with CFR-6 showed high effectiveness factors such as were obtained with CFR-5 but with much less linear range.

CFR-7. CFR-5 was modified to have a concave cambered rudder with thickened, squared trailing edge, which was used to facilitate the model change. The results given in Fig. 32 indicate that CFR-7 has slightly less linear range than CFR-5 but more than CFR-6.

The results of these tests showed that airfoil section shape and particularly the shape of the rudder must be designed according to best airfoil section information. A concave rudder with a sharp trailing edge appears to give the linear effectiveness factor over a large range of angles of yaw, probably because the hinge-moment curve slope is linear over a larger range of rudder angles.

Data and calculations. Data showing the effectiveness of the coupled fin and rudder were obtained as follows:

1. Curves were obtained of side force vs angle of yaw for constant fixed-rudder angles throughout the range to be used (cf. Fig. 30).

FIGURE 31

SIDE FORCE VS. YAW

GER-5

(FAIRED INTERSECTION - SQUARED T.E.)

SYM.	$\frac{V_1}{V}$	$\left(\frac{d\Delta C_Y}{d\Delta\alpha_{OT}}\right) / \left(\frac{d\Delta C_Y}{d\Delta\alpha_{OT}}\right)_{FIXED}$
x	FIXED	1.0
▽	11.65	1.3
□	8.88	2.1
△	7.22	3.8
○	6.61	4.8
◇	6.40	7.8

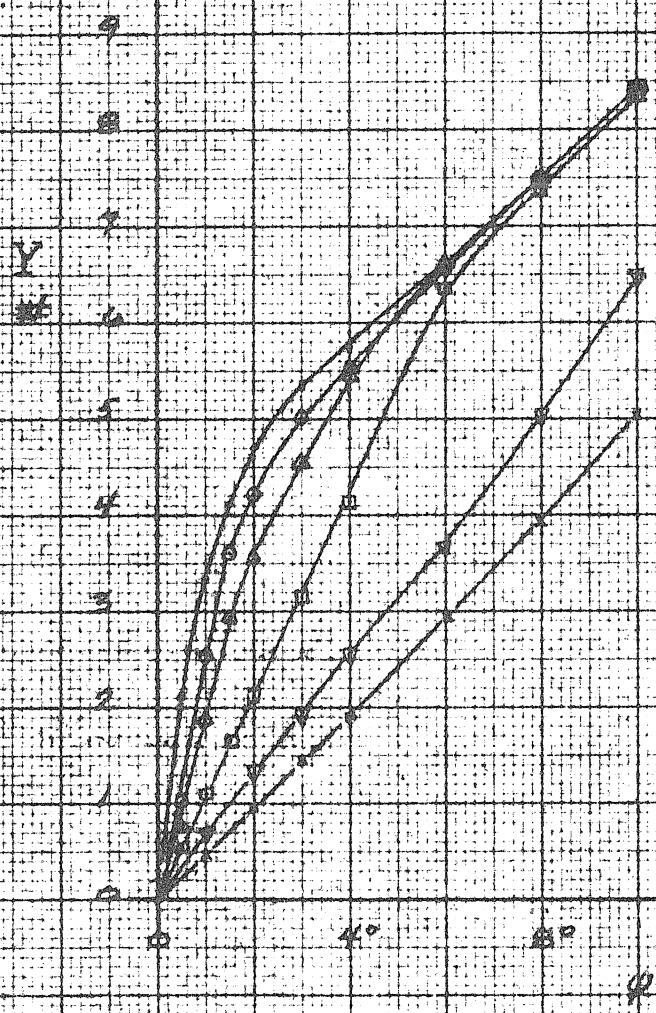

FIGURE 32

SIDE FORCE VS. YAW

CER-7

(CONCAVE SIDED RUDDER)

(THICK SQUARE T.E.)

SYM	q/α	$\left(\frac{\Delta C_Y}{\Delta \psi_0}\right) / \left(\frac{\Delta C_Y}{\Delta \psi_0}\right)_{FIXED}$
x	FIXED	1.0
•	7.22	2.5
o	6.05	5.13

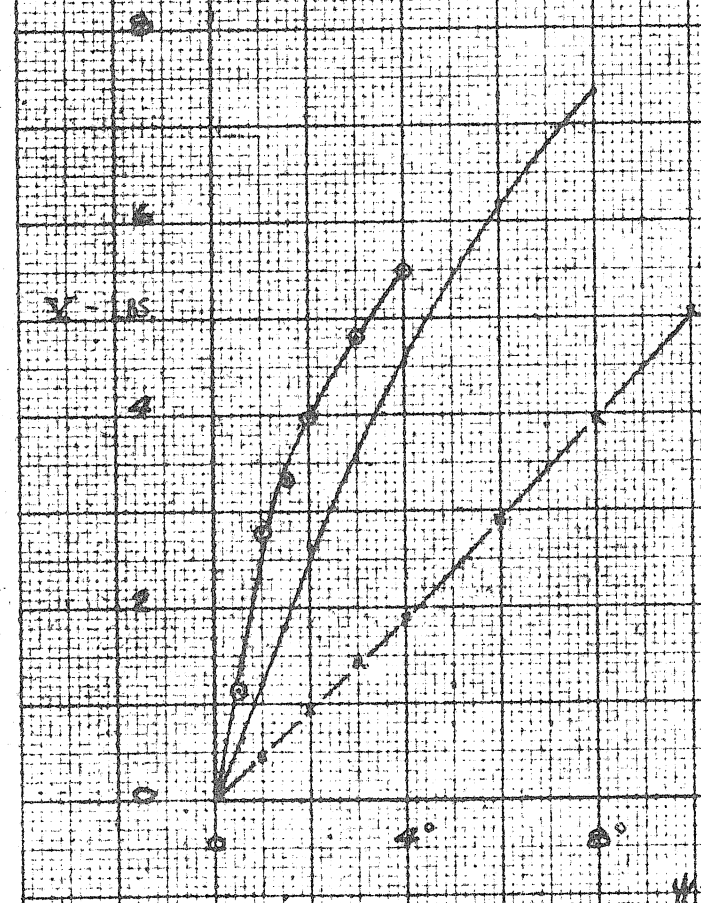

2. With various constant coupling ratios, the rudder angles corresponding to various yaw angles were observed. These observations were made for positive and negative angles of yaw to $\pm 15^{\circ}$. In order to allow for slight asymmetry, corresponding rudder angles on both sides were averaged and the calculations made from the average value. The model and testing equipment was adjusted to give zero rudder at zero yaw.

3. The side force C_L was determined by reading the side force corresponding to the angle of rudder and yaw as noted experimentally from Fig. 30.

The experimental results for CFR-5 and CFR-7 are shown in Figs. 31 and 32, respectively.

Check of static stability theory. A check of the elementary theory given (cf. Fig. 27) was made as follows (this method of checking made it possible to compare the correspondence of theory and experiment with a minimum of required data:

1. Fig. 31 gives the coupling ratio 1/R and the effectiveness ratio.

$$\eta_s = 1 + \tau \frac{\beta}{\psi} = \left(\frac{dC_L}{d\psi}\text{ Coupled}\right) \Big/ \left(\frac{dC_L}{d\psi}\text{ Fixed}\right)$$

2. The coupling ratio coefficient R_s/R corresponding to each experimentally measured effectiveness ratio is read from the theoretical curve on Fig. 32.

3. From this value is calculated the coupling ratio R_s which would give the singular point.

4. If the theory is consistent with experiment, then all such calculated coupling ratios R_s giving the singular point should be equal.

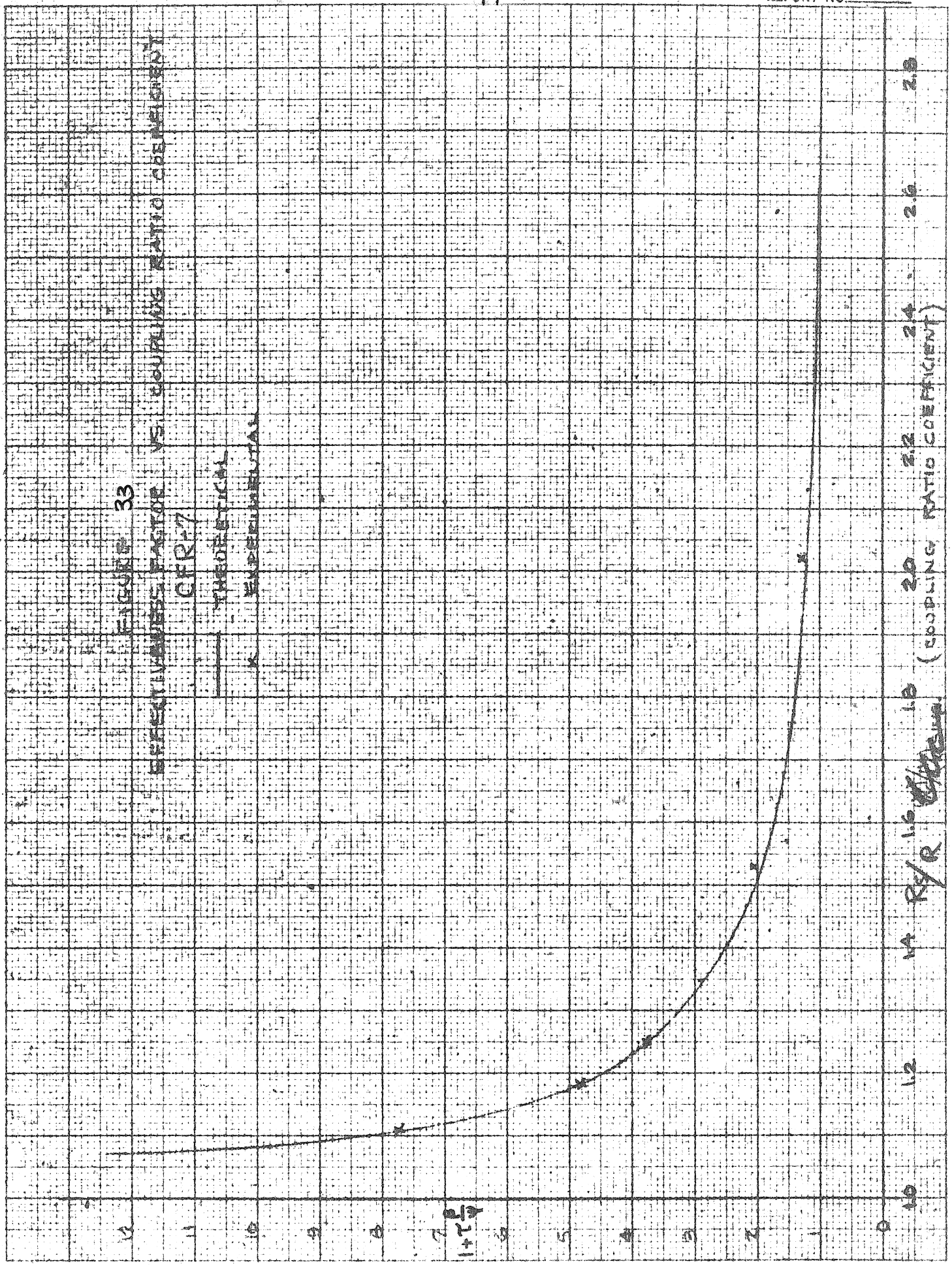
EFFECTIVENESS FACTOR VS COUPLING RATIO COEFFICIENT
GFR-7
THEORETICAL
EXPERIMENTAL
K
Rf/R
(COUPLING RATIO COEFFICIENT)
1.2
1.4
1.6
1.8
2.0
2.2
2.4
2.6
2.8
0
1
2
3
4
5
6
7
8
9
10
1+2β

FIGURE 33

5. Using the average of all calculated values of R_s, the coupling ratio coefficient and the effectiveness ratio are plotted as experimental points on Fig. 33, which shows that, after locating the singular point, the effectiveness ratio or factor for all other coupling ratios or ratio coefficients (R_s/R) may be determined over the range from less than 1.05 and greater than 2.0. The tail efficiency η_s extends from 1.0 to greater than 8.0.

D. Dynamic Stability Tests

The foregoing results appeared to indicate that the coupled fin and rudder could be designed from the standpoint of statics. Because of the difficulty experienced regarding flutter when the original models were tested in the 5-foot tunnel, it seemed advisable to study the dynamic aspects of the coupled fin and rudder.

Dynamic tests were made on CFR-8 to determine the behavior of the coupled tail under conditions similar to free-flight conditions on the airplane. The results of these preliminary tests on a dynamic model (cf. Table VIII) showed that, by correctly adjusting the aerodynamic mass constants, a directional-stability device was obtained which had dynamic stability, together with a restoring moment much larger than ordinary types of rudders. A very important feature is that the particular design and adjustment which gave stability and damping also operated as an anticipatory automatic control rudder. Such a design is therefore a mechanical device which reacts properly to side accelerations as well as to yaw displacements and angular velocities. A device of this type may prove to be a very definite advance in fin and rudder design.

CFR-1 was reworked to give CFR-8. The airfoil section was modified

to have a slightly concave rudder surface. The trailing edge was similar to the rounded trailing edge of CFR-2 but had a much smaller radius, thus simulating a squared trailing edge. The model was approximately 1/4-scale and with the horizontal tail weighed about 6 pounds. The fin and rudder weighed about 2 lb/sq ft and therefore was nearly twice as heavy in proportion as normal airplane controls.

This empennage model was mounted in the tunnel as a wind vane. The c. g. of the tail was located 3 feet aft of freely operating ball bearings.

With the original mass-balance condition, the coupled fin and rudder oscillated rather violently with amplitudes of $\pm 20^{\circ}$ yaw and periods of 1.5 seconds. Placing restoring springs on the oscillating system and varying the air speed had little noticeable effect on the period. The coupling ratio affected the amplitude of oscillation. For a coupling ratio giving an effectiveness factor of 1.0, the rudder did not build up in oscillation and, if disturbed from equilibrium, damped out rapidly. With the rudder connected as a conventional rudder and floating-freely, oscillations were damped out but not as rapidly as with the rudder fixed. The coupled fin and rudder did not oscillate when at zero yaw but, if displaced 3 or 4 degrees, built up to a steady oscillatory state.

The oscillation is better described as a directional dynamic instability. The mass distribution for the oscillatory cases was such that the rudder was considerably underbalanced.* Observation of the model during oscillation showed that the circumstances causing the oscil-

* Although the c.g. of the entire tail was above the tip hinge line, the centroid with respect to the obtuse node line was sometimes below the node line (cf. App. B), giving the wrong inertia effect and causing dynamic instability.

lation are as follows:

1. Because of the increased effectiveness the side force produced by the coupled fin and rudder gives a much greater directional restoring moment.
2. Because of the yawing velocity $\dot{\psi}$, when the fin is geometrically at a yaw angle equal to $\dot{\psi} x/U$, aerodynamically it is at zero yaw (x is tail length, U is air velocity).
3. From observations of the dynamic model, it is noted that the rudder lags sufficiently so that, when the fin passes through geometric zero, the rudder is deflected to increase the velocity in yaw at zero yaw rather than to decrease it.
4. It is also apparent that the mass distribution is such as to tend to make the rudder lag because of the acceleration as the rudder returns from maximum amplitude.

By raising the c.g. of CFR-8, it was found that the phase could be shifted so that the rudder damped out and did not oscillate.

E. Correlation of Final Dynamic Stability Theory with Tests

Before the stability theory was developed in any complete form, dynamic wind-tunnel tests were conducted on swinging arms with two different model tail surfaces and many different balance conditions. When the final stability criteria were used to predict, by analysis, the behavior of these models in the dynamic tests, the results were as shown in Table IX. Of the nine cases which were studied, the final stability criteria gave the correct indication in every case. Four out of nine of the configurations were stable.

Table IX

Correlation of Dynamic Stability Criteria with Tests

	1S	2S	3S	4S	5S	6S	7S	1L	2L
z	-6.6	-3.9	(+2.9)*	(+1.7)*	(+0.7)*	-0.10	-0.7	-0.18	(+0.30)*
R	.115	.095	.072	.095	.115	.161	.072	.167	.143
z_β **	+3.2	+1.5	+3.2	+1.5	+0.5	(-0.7)	+3.2	(-.4)	+.2
$z - z_\beta$	-9.8	-5.4	-0.3	(+0.2)	(+0.2)	(+0.6)	-3.9	(+.22)	(+.10)
x_β/R	-4.6	-5.5	-7.4	-5.5	-4.6	-3.3	-7.4	-3.0	-3.5
$\frac{z - z_\beta}{x_\beta/R}$	2.1	1.0	.04	-.036	-.043	-.197	-.53	-.07	-.03
z/x	.184	.108	-.08	-.048	-.019	+.003	+.019	.002	-.004
z_α	-1.20	-0.60	+0.44	-0.60	-1.20	-2.0	+0.44	-2.1	-1.8
η_D	0.43	0.39	+9.3	(-10.5)	(-8.5)	(-4.5)	0.72	(-7.7)	(-20.6)
Stability*** Prediction	S	S	S	U	U	U	S	U	U
Actual Test	S	S	S	U	U	U	S	U	U

*U unless $\eta_D > 0$, in which case S.

** h_β/τ = .18; R_S = .13 for S
= .27; = .15 for L (cf. Ref. 1, Table 2)

*** U = Unstable, with reason shown in ( ). S = Stable.

Itis interesting to note that all cases of instability were due either to static instability $z_\beta < 0$, $\eta_S < 0$, or to dynamic instability $z > 0$, $\eta_D < 0$; and normally the instability was indicated simply by $z_\beta < 0$ or $z > 0$ (cf. Eqs. 8). In 3S , the one exceptional case where the $z > 0$ failed to predict instability, the more general rule $\eta_D > 0$ gave the correct prediction. The present theory therefore provides a simpler and more accurate stability criterion than that previously developed (cf. Ref. 1). Further tests would be desirable to confirm the analytical work under more carefully controlled test conditions, with higher values of η_D , and with more accurate determination of R and R_S by experiment. It is noteworthy that the present analysis agrees perfectly with test data and observations which were obtained six years ~~previously~~ before, which seems to further strengthen one's confidence in the principle of coupled surfaces, and the regularity with which they conform to certain well defined rules.